Atmospheric Chemistry and Physics
Discussions
Open Access
EGU

Atmospheric processes affecting the separation of volcanic ash and SO$_2$ in volcanic eruptions:

Inferences from the May 2011 Grímsvötn eruption

Fred Prata[1], Mark Woodhouse[2], Herbert E. Huppert[3], Andrew Prata[4], Thor Thordarson[5], and Simon Carn[6]

[1]Visiting scientist, Department of Atmospheric, Oceanic and Planetary Physics, Clarendon Laboratory, University of Oxford, UK

[2]School of Mathematics, University of Bristol, Clifton, Bristol, UK

[3]Institute of Theoretical Geophysics, Department of Applied Mathematics and Theoretical Physics, University of Cambridge, UK

[4]Department of Meteorology, University of Reading, Earley Gate, Reading, UK

[5]Faculty of Earth Sciences, University of Iceland, Reykjavik, Iceland

[6]Department of Geological and Mining Engineering and Sciences, Michigan Technological University, Houghton, MI, USA

Correspondence to: Fred Prata (fred_prata@hotmail.com)

Abstract. The separation of volcanic ash and sulphur dioxide (SO$_2$) gas is sometimes observed during volcanic eruptions. The exact conditions under which separation occurs are not fully understood but the phenomenon is of importance because of the effects volcanic emissions have on aviation, on the environment and to the earth's radiation balance. The eruption of Grímsvötn, a subglacial volcano under the Vatnajökull glacier in Iceland during 21–28 May 2011 produced one of the most spectacular examples of ash and SO$_2$ separation that led to errors in the forecasting of ash in the atmosphere over northern Europe. Satellite data from several sources coupled with meteorological wind data and photographic evidence suggest that the eruption column was unable to sustain itself, resulting in a large deposition of ash which left a low level ash-rich atmospheric plume moving southwards and then eastwards towards the southern Scandanavian coast, and a high level predominantly SO$_2$ plume travelling northwards and then spreading eastwards and westwards. Here we provide observational and modelling perspectives on the

5

separation of ash and SO$_2$ and present quantitative estimates of the masses of ash and SO$_2$ erupted, the directions of transport, and the likely impacts. We hypothesise that a partial column collapse or perhaps several occurred during the early stage of the eruption leading to an ash-laden gravity intrusion that was swept southwards, separated from the main column. Our model suggests that water-mediated aggregation caused enhanced ash removal because of the plentiful supply of source water from

5 exsolved magmatic water, from melted glacial ice and from entrained atmospheric water. The analysis also suggests that ash and SO$_2$ should be treated with separate source terms, leading to improvements in forecasting the movement of both types of emissions.

1   Introduction

Vigorous volcanic eruptions emit copious amounts of gases and particles into the atmosphere where they are transported by the

10 winds, potentially in all directions. They can be transported rapidly zonally as in the case of the eruption of Puyehue-Córdon Caulle, southern Chile during June 2011 where ash and SO$_2$ travelled together circling the southern hemisphere at latitudes south of 30 °S. They can be transported vertically by air circulations as in the case of Nabro, Eritrea also in June 2011 where the monsoon circulation may have played a part in lifting SO$_2$ gas into the stratosphere (Bourassa et al., 2012), although Fromm et al. (2014) provides a convincing case for direct gas injection. Prevailing atmospheric winds can play a pivotal role in the

15 transport of ash and SO$_2$ as in the case of the April and May 2010 eruptions of Eyjafjallajökull, Iceland, during which large amounts of ash were transported zonally and meridionally over continental Europe leading to major disruptions of air traffic. The direction of transport is determined by the strength and direction of the zonal and meridional wind fields and these vary with height. Vertical wind shear varies with location and time and is commonplace.

SO$_2$ gas and ash particles represent two major components of vigorous volcanic activity and these may be emitted together

20 or individually and this mix can and does vary with time, due largely to the character of the volcanic activity and the geological setting of the volcano. Since there is no guarantee that ash and SO$_2$ will be erupted at the same time, nor that they will remain collocated in space and time, there is a good reason to investigate the conditions under which these emissions remain together and conditions under which they separate. Separation has been observed during the eruptions of Okmok and Kasatochi (Prata et al., 2010), this Grímsvötn eruption (Moxnes et al., 2014) and during the Eyjafjallajökull eruption (Thomas and Prata, 2011),

25 although collocated transport is also often observed. Holasek et al. (1996) investigated ash and gas separation through analogue laboratory experiments. They found that gas and ash separation occurred through buoyancy effects with particle sedimentation leaving higher gas concentrations above. Separation can also occur when ash and SO$_2$ are emitted in separate explosive events, where either the energy of the eruption has changed, emplacing the materials at different heights, or the atmospheric conditions have changed in the intervening period. These processes are complex and difficult to predict for individual events.

30 Here we study the remarkable separation of SO$_2$ and ash during the 21–28 May, 2011 eruption of Grímsvötn, using mostly satellite data but also ground based remote sensing measurements and model simulations. The separation was the greatest possible. SO$_2$ reached high altitudes (>10 km), travelled northwards and then spread eastwards and westwards, while the ash remained at low altitudes (<4 km) travelled southwards, before spreading eastwards, eventually reaching the western coast of

Norway. The separation led to a poor forecast of the ash hazard to aviation and we suggest how such errors can be avoided in the future.

The injection of SO_2 into the stratosphere, and its subsequent conversion to sulphate aerosol is important for understanding the radiative impact of volcanic eruptions (Robock, 2000). If the SO_2 emission remains largely in the troposphere its potential
5   impact on radiative forcing is less, because the residence time of the resulting sulphate aerosol is shorter. Stratospheric sulphate aerosols on the other hand can potentially alter the radiative balance. It is shown here that the Grímsvötn SO_2 did indeed penetrate into the stratosphere. The satellite data are used to estimate the total SO_2 injected into the stratosphere, and the total mass of fine ash injected into the lower troposphere.

Our paper stresses the importance of a multidisciplinary approach to the study of volcanic eruptions on the atmosphere:
10   volcanolgical insights, space-based observations, dispersion modelling and fluid dynamics are all required to develop understanding of the dominant processes involved. The paper is organised as follows. The chronology of the eruption and important events are described, followed by a short section on the transport and the tools used to determine it. Next the satellite data are introduced and estimates of the ash mass loading, the SO_2 amount, cloud-top temperature and height are provided. The phenomenon of particle-gas separation is discussed and observational evidence is presented for the Grímsvötn eruption. An
15   uncoupled plume model, in which plume dynamics and plume microphysics are examined separately is used to provide insights into the most significant processes relevant to particle-gas separation. Most of the satellite observations and some modelling results are included as Supplementary Material. The main inferences from the study are presented in a concluding discussion section and an Appendix provides a mathematical description of the plume model employed.

2   Chronology of the Grímsvötn eruption

20   Grímsvötn is a subglacial volcano situated under the Vatnajökull glaicier in south-eastern Iceland. Like many Icelandic volcanoes it has a long record of eruptive activity (Thordarson and Larsen, 2007) with the last notable event prior to the May 2011 activity occurring between 1–6 November, 2004. On the afternoon of 21 May 2011 at around 17:30 UTC, seismicity and thermal anomaly measurements at Grímsvötn indicated that an eruption was likely, and at 19:00 UTC the eruption penetrated the Grímsvötn subglacial caldera. First signs of a plume entering the atmosphere were recoded by the Spin-Enhanced Visible
25   and Infra-Red Instrument (SEVIRI) on board the geostationary Meteosat Second Generation (MSG)-2 satellite at 19:15 UTC on 21 May. The weather conditions at the start of the eruption were good and photographs of the plume (see Fig. 1) as it emerged out of the glacier clearly showed an ash laden plume reaching several kilometres into the atmosphere. As evening fell, visibility worsened and cloud also moved in from the north making visual identification of the plume difficult. Early reports and some later analysis suggested that the plume had reached perhaps 20 km. Ashfall was evident all around Grímsvötn and
30   was reported from the Reykjavik area in the SW to Tröllaskagi Peninsula in the north. Figure 2 shows a map of the region indicating the location of Grímsvötn, some of the towns and the airport.

According to the status reports (http://earthice.hi.is/grimsvotn_eruption_2011) issued by the Icelandic Meteorological Office (IMO) and the Institute for Earth Sciences (IES) in Iceland, the column reached greatest heights during 21–22 May which were

Figure 1. The changing appearance of the Grímsvötn eruption column in photographs taken at the start of the eruption in clear skies at 20:00 UTC (18:00 local time) (top), and later in a dark, cloud-laden atmosphere (bottom). There is a clear indication (lower photograph) of ash in the lower parts of the column. Later photographs show mammatus clouds forming in the eruption cloud suggesting ice nucleation and this may have contributed to a more rapid loss of ash particles from the cloud.
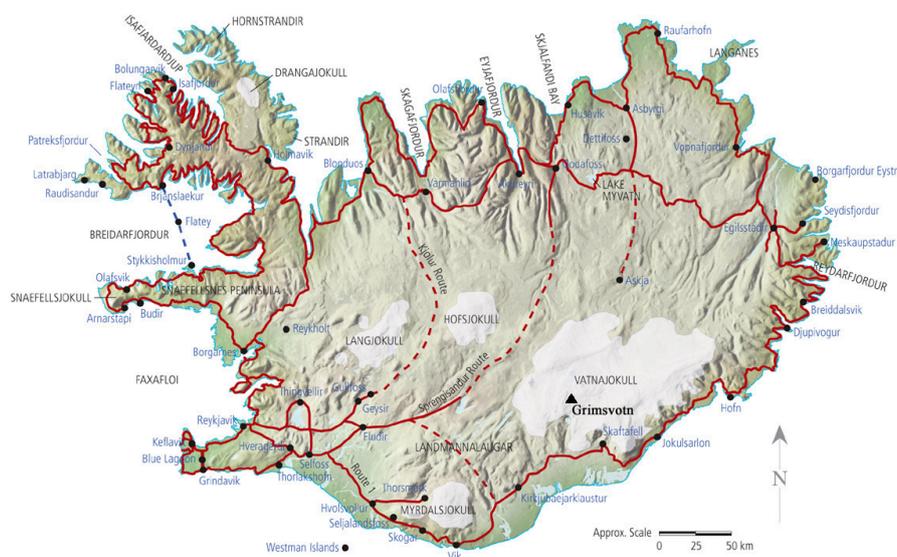
Figure 2. Map of Iceland showing towns, the road network and the location of Grímsvötn.

estimated to be between 15–19 km. Subsequently the columns reached 10 km and then by 26 May did not exceed 8 km and mostly remained below cloud level at 5–6 km. The Grímsvötn eruption is believed to be the largest in Iceland since the eruption of Katla in 1918, and erupted approximately $\sim$0.7 km^3 (Gudmundsson et al., 2012a) of tephra in about 2 days compared with the April-May 2010 Eyjafjallajökull which erupted $\sim$0.27 km^3 over a 39 day period (Gudmundsson et al., 2012b). Stevenson

5   et al. (2012) demonstrated that ash from Eyjafjallajökull reached many parts of the United Kingdom, noting that even quite large ($>$50 μm radii) particles were collected on the ground. The much larger Grímsvötn eruption was expected to send more ash towards Europe than the April-May 2010 Eyjafjallajökull event that caused Europe-wide aviation disruption.

3   Transport

Atmospheric dispersion models are used to simulate the transport of volcanic ash in the atmosphere–so-called Volcanic Ash

10   Transport and Dispersion (VATD) models (e.g. HYSPLIT, Draxler and Rolph (2003)). These models have been quite successful for both small (e.g Eyjafjallajökull) and mid-size (e.g. Puyehue-Córdon Caulle) eruptions. They depend for their accuracy on the precise details of the eruption parameters, and in particular on being able to specify the mass eruption rate (MER), its vertical structure and its temporal variation. If these are incorrect then the forecast dispersion is also incorrect. Many VATD models rely on an estimation of the MER obtained from a parameterized relationship between the MER and the height of the

15   eruption column. The most commonly used has the MER proportional to the fourth power of the height (Sparks et al., 1997b; Mastin et al., 2009). There are two significant consequences for forecasting the transport if the height is in error. First, for

an atmosphere with significant wind shear where the height is incorrectly specified, the transport will be incorrect. Second, as the MER depends strongly on height, the estimated amount of ash may be significantly under- or over-estimated, if the height is under- or over-estimated. More sophisticated models of the MER are available (Mastin et al., 2009), and recent work by Woodhouse et al. (2013b) has shown a dependence of the MER on wind shear for bent-over plumes. These more detailed

5 treatments also require more detailed observations of various parameters to specify the MER.

HYSPLIT ash dispersion runs using GDAS wind fields were used to test the sensitivity of the transport to the height of the eruption column during the Grímsvötn eruption. For a column rising to 30,000 ft beginning on 21 May at 19:00 UTC the transport of ash is mostly northwards and then spreads eastwards and westwards. Conversely, for ash emitted to a height of 10,000 ft on 22 May at 14:00 UTC the transport is mostly southwards and then eastwards towards Scotland and on to the

10 southern part of Scandanavia. These two scenarios are motivated by satellite observations of volcanic emissions taken by polar and geostationary instruments (see next section) and are therefore indicative of what actually happened. During the event, the London Volcanic Ash Advisory Centre (VAAC), among others, forecast ash emissions towards the north and south, in broad agreement with the HYSPLIT simulations. As we shall see, the forecast of significant ash emissions to the north was incorrect because these emissions were almost entirely SO_2 gas, and the forecast overestimated the amount of ash transported to the

15 south and then eastwards, probably due to an incorrectly specified vertical distribution of ash at the source.

A more complex model written specifically for volcanic ash eruptions, FALL3D (Folch et al., 2009) was also used to study the transport. The model is an Eulerian dispersion model which includes several different parametrisations that can used to specify the source term. It is driven by input atmospheric wind fields and has been used in many studies of atmospheric transport of ash, particularly to investigate ash fall. We used FALL3D initialised with NCEP wind fields at 6-hourly intervals

20 starting at 19:00 UTC on 21 May 2011. The source term was specified using one of the pre-set options, in this case a point source and the plume options were used. A forward run was performed on a grid of 0.2 x 0.2 degree resolution, with a vertical scale of ∼0.1 km for a total duration of up to 96 hours. Here we are not concerned with testing the model's propensity to accurately simulate long-range ash transport, but rather to investigate the hypothesis that the source of ash was from a column collapse, with the ash injection treated as an impulse. Some of the results of the simulations are shown in the Supplementary

25 material section (Figure S1), at 6-hourly intervals starting at 13:00 UTC on 22 May. Here we summarise the main findings, noting that FALL3D is used for ash forecasting and so the results are 'typical' of what is found from using state-of-the-science VATD models.

The short duration of the source of ash results in a small plume or cloud of ash dispersing to the SSW and then turning southwards (Fig. S1) and later towards the east (not shown). The ash eventually is transported over the northern part of the

30 United Kingdom, somewhat south of the path observed in SEVIRI, and then onto the southern part of Scandanavia, where ground-based particle measurement stations recorded elevated levels of PM10 (Prata and Prata, 2012). The FALL3D simulations also show a small amount of ash transported towards the north-west at higher levels, collocated with satellite observations of SO_2. This ash cloud, also observed in ash retrievals from SEVIRI, the Infrared Atmospheric Spectrometer Interferometer (IASI) and Moderate Resolution Spectroradiometer (MODIS), is short-lived and has dissipated by 20:00 UTC on 22 May.[1]

---

[1]Here it may be assumed that the ash is still in the atmosphere but of a concentration too low to be detected by current satellite infrared measurements.

The initial amount of erupted fine ash required to generate an ash cloud consistent with the satellite observations cannot be modelled using the fourth power law, as this produces almost 100 times too much fine ash. An approach more consistent with the satellite estimates is to assume a much lower amount of erupted ash spreading outwards as a gravitational current from a collapsing part of the eruption column. FALL3D is not currently configured to simulate this kind of source term (areal), so the source term was scaled to match the satellite retrievals, assuming a maximum height of 6 km and with a suitable vertical distribution of ash. The MER scales as H^4, where H is the column height, so the MER is reduced by a factor of ∼100 if the column height is reduced from 19 km to 6 km.

4 Satellite data analyses

Satellite instruments have been used extensively to monitor volcanic emissions (Prata, 2009). Both ash and SO_2 gas can be quantified using measurements made in the infrared (e.g. Clarisse et al., 2010; Prata and Prata, 2012; Carn et al., 2005), and in the ultraviolet, (e.g. Carn et al., 2016), while UV-visible reflected light can be used to identify volcanic aerosols (aerosol optical depth) and passive microwave measurements can be used to detect large (mm-sized) volcanic particles. These passive measurements have been recently supplemented by an active space borne lidar that can provide much needed vertical information. The Cloud-Aerosol Lidar with Orthogonal Polarization (Caliop) on board the CALIPSO polar-orbiting platform provides vertical structure information from backscattered light, along the sub-satellite point but has a long repeat cycle which inevitably means limited coverage for rapidly evolving, spatially limited events such as low to medium size volcanic eruptions. Table 1 provides a list of the satellite instrument data used in this study including the salient characteristics of these instruments.

4.1 Cloud-top height

An estimate of the column height of eruptive material is critical to understanding the movement of ash away from its source. Initial estimates of the height of the ash column, based on radar measurements by the IMO (Petersen et al., 2012), suggested that it had reached ∼20 km. However, the satellite data analysed here, together with radiosonde temperature profiles made at Keflavik airport, indicate that the column maximum height did not exceed ∼16 km and varied between ∼8 km and ∼16 km from onset at 19:00 UTC on 21 May 2011 until probable collapse sometime after 05:15 UTC on 22 May.

At the start of the Grímsvötn eruption a tall and optically thick column extended several kilometres into the atmosphere. During this phase, the large opacity of the cloud makes ash retrieval using infrared and ultra-violet radiation very difficult. Particle sizes are large (mm to cm size) and hot gases, principally water vapour and CO_2 dominate the emissions. The evolution of the column can be studied using single-channel infrared measurements (Fig. 3), by making the assumption that the cloud is behaving as a blackbody and the brightness temperatures correspond to the cloud-top temperature. The blackbody assumption is generally quite good, but because the cloud may overshoot, undercooling may occur (Woods et al., 1995) leading to cloud tops with IR temperatures many degrees Kelvin below the background atmospheric temperature. Radiosonde data from Keflavik airport (see map Fig. 2) were used to relate the IR brightness temperatures to cloud top height. The radiosonde data show a tropopause at ∼8.5 km and a dry layer between 3–4 km. The winds show easterlies up to about 4 km, then westerlies up to

Atmospheric
Chemistry
and Physics
Discussions

Table 1. Satellite instruments used in this study to identify volcanic emissions. The instruments are: AVHRR–Advanced Very High Resolution Radiometer; MODIS–Moderate resolution Infrared Spectroradiometer; AIRS–Atmospheric Infra-Red Sounder; IASI–Infrared Atmospheric Spectroradiometer Interferometer; SEVIRI–Spin-stabilised Enhanced Visible and Infra-Red Instrument; OMI–Ozone Monitoring Instrument; Caliop–Cloud-Aerosol Lidar with Orthogonal Polarisation.

Instrument/Platform	Spatial resolution (km^2)	Temporal resolution (hours)	Parameter
AVHRR/Meto-A, B	~1.1x1.1	~3	Ash
MODIS/Terra/Aqua	0.25x0.25–1x1	~6	Ash/SO_2
AIRS/Aqua	~13x13	~12	SO_2/Ash
IASI/Metop-A	~10x10	~12	SO_2/Ash
SEVIRI/MSG-2	~3x3–10x10	0.25	Ash
OMI/Aura	~12x12	24	SO_2/AAI
Caliop/CALIPSO	~0.1x0.3	16 days	Aerosols

the tropopause and high level winds from the south. A tall column of ash entering this highly sheared atmosphere will suffer transport in at least three different directions. Plume evolution can also be estimated from spatial changes in the brightness temperature images and is a useful way to identify the onset of column growth.

The shadow cast by the Grímsvötn eruption clouds seen on some MODIS images can also be used to estimate cloud top height (Prata and Grant, 2001). A MODIS/Aqua 250 m resolution image acquired at 13:15 UTC on 22 May shows the Grímsvötn column with a strong shadow cast onto the ground and cloud below (Fig. 4). Utilising the geometry of the satellite and sun viewing directions and the contrast difference between the dark shadow and brighter cloud/ice below, the highest parts of the ash column in this image are estimated to be 16±1 km, with other parts of the column having lower tops. It can also be seen that there is an ash layer to the south of the column that appears to be detached and dispersing southwards. This ash layer may have arisen from a less vigorous phase of the eruption (when the column top was lower) or possibly was formed from partial column collapse. Whatever the exact mechanism involved, this ash layer is effectively independent of the ash fed into the column at source and could therefore be treated as a separate source for the purpose of forecasting its movement. The layer is evident on later MODIS images (see later Fig. 8) and it is this low-level ash layer that eventually travels eastwards towards Scotland and on to south-western Scandanavia.
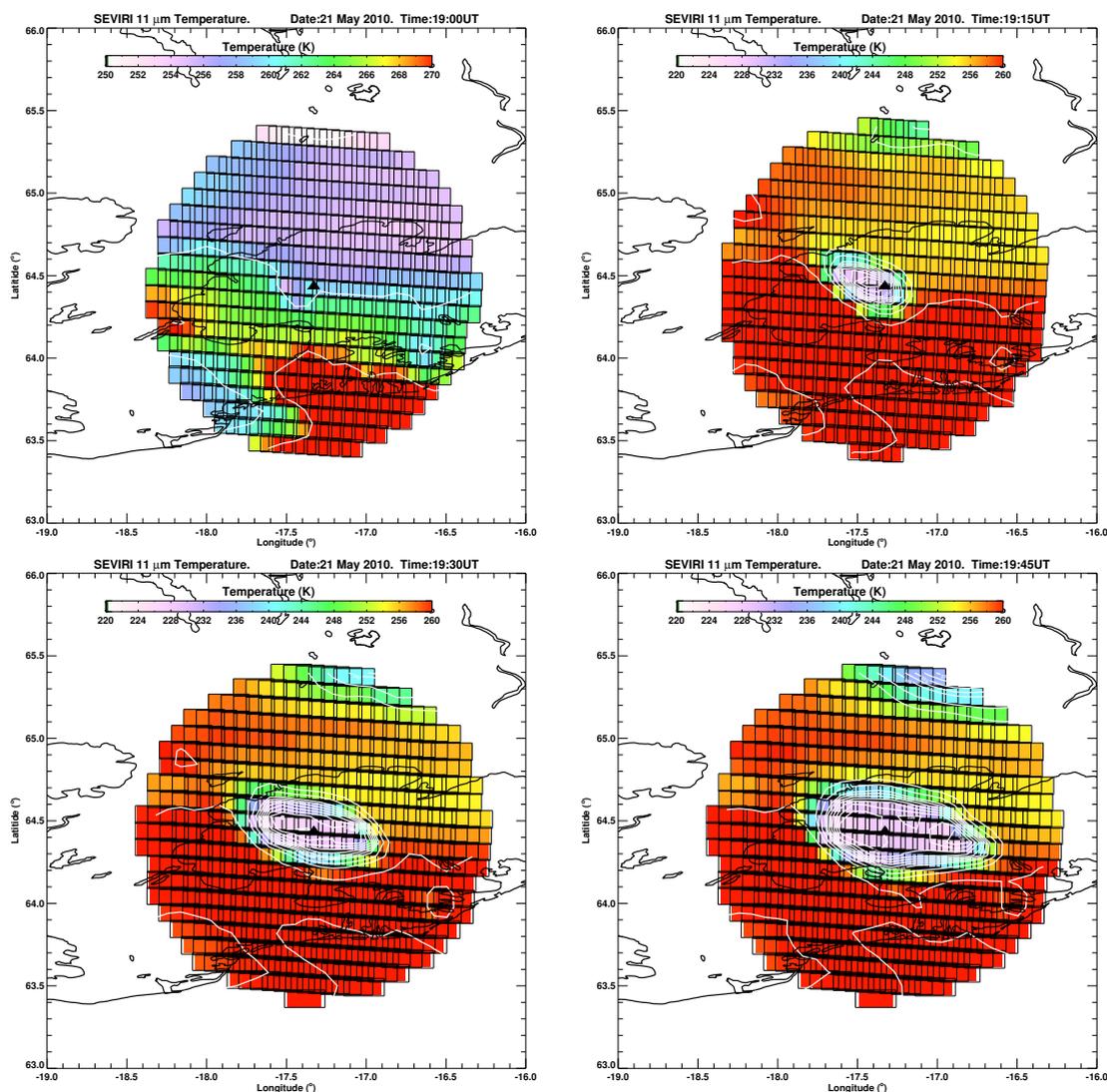
Figure 3. Close-up views of the 11 μm brightness temperatures from the SEVIRI instrument at 15 min intervals, starting at 19:00UT on 21 May 2011. The rapid plume rise may be interpreted by the change in extent of the cloud top temperatures. There is no evidence of an eruption on the image at 19:00 UTC. The location of Grímsvötn is shown as a black triangle.

4.2 Spaceborne lidar measurements

The CALIOP instrument on board the polar orbiting CALIPSO platform is a polarization-sensitive, elastic backscatter lidar capable of providing high vertical resolution (∼60 m) attenuated backscatter profiles of clouds and aerosols, and cloud-top heights. The instrument transmits linearly polarized light and measures the return signal at 532 and 1064 nm. The components

5   perpendicular and parallel to laser polarization are measured separately at 532 nm. Details of the instrument, the science
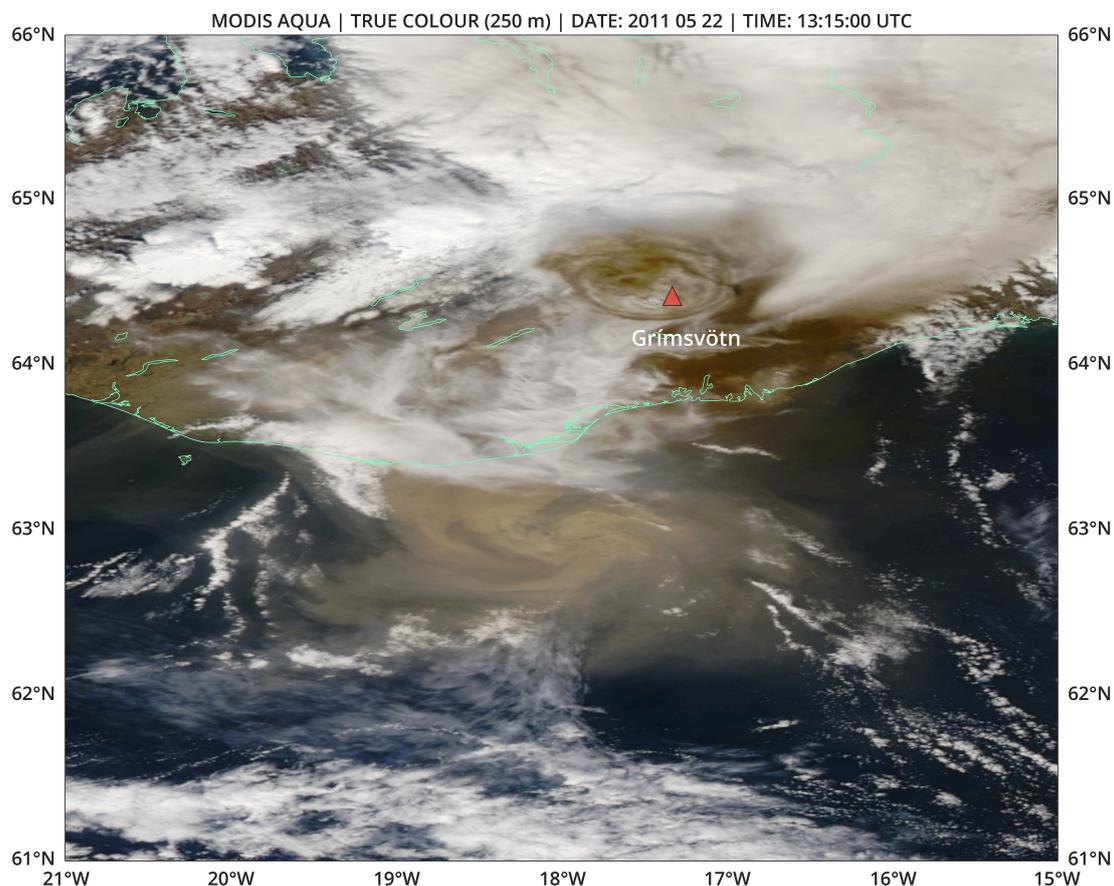
Figure 4. MODIS true-color 250 m resolution image of the Grímsvötn eruption column, showing the shadow cast on the ground and cloud below (to the N of the column). Note also the the ash layer off the south coast that appears detached from the main column, suggesting that it is no longer being fed by ash from the vent. *Image: MODIS/Aqua, 22 May 2011, 13:15 UTC.*

applications and an example of its use in a volcanic study may be found in Hunt et al. (2009), Vaughan et al. (2009) and Winker et al. (2012). The lidar is near-nadir pointing, has a ground footprint diameter of 70 m and a repeat time of 16 days, which limits the number of times the lidar beam coincides with a target of interest. Ten CALIOP coincidences were identified for the Grímsvötn ash and SO_4^{2-} clouds between 21–23 May, 2011. Figure 5 shows an example of a CALIOP pass on 23

5   May when the CALIPSO trace intersected an ash cloud to the south of Iceland and a SO_4^{2-} layer to the north. The upper left-panel shows indices based on coincident AIRS brightness temperature difference measurements, using an index to indicate ash (orange/red colours) or SO_2 (shades of blue). Details of the ash and SO_2 indices can be found in Prata et al. (2015) and Hoffmann et al. (2014), respectively. The upper-right panel (Fig. 5b) shows a MODIS/Aqua true-colour image acquired at the same time as the AIRS measurements.Panel (c) shows the CALIOP attenuated backscatter signal measured at 532 nm.

10 The black horizontal line indicates the height of the tropopause determined from GMAO (Global Modelling and Assimilation

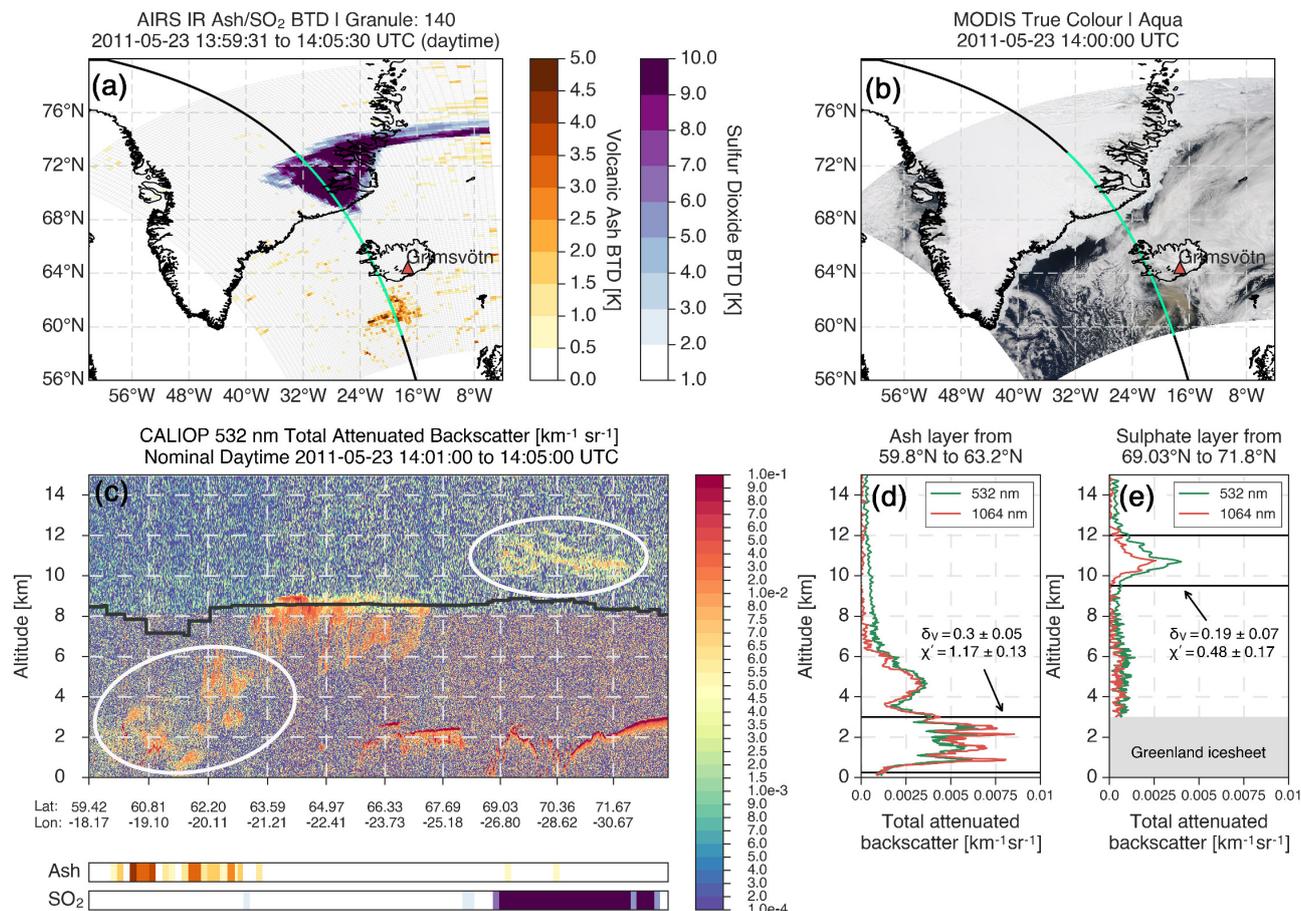Atmospheric
Chemistry
and Physics
Discussions

Figure 5. *Top-panels*, (a): AIRS brightness temperature difference for volcanic ash (yellow/ornage/red) and AIRS brightness temperature difference for SO$_2$ (shades of blue). The trace of the CALIPSO satellite is indicated by the black/green line, where the green-colored portion of the line indicates the region of overlap between the Caliop and AIRS image data. (b) MODIS/Aqua true-colour image showing the low-level ash cloud (brown). *Bottom-panels:* (c) Caliop backscatter curtain for 532 nm light with the ash and sulphate layers indicated by the white-coloured ellipses. The lower strips show temperature differences based on the AIRS data indicating regions affected by ash and SO$_2$ gas. Panels (d) and (e) show vertical profiles of backscatter for ash and SO$_4$$^{2-}$, respectively. δ_v is the volume depolarisation ratio and χ' is the colour ratio. Date and time of overpass: 23 May 2011, 14:01–14:06 UTC.

Office) reanalysis data (Rienecker et al., 2008). The strips at the base show collocated AIRS pixels along the CALIOP track where ash and SO$_2$ have been identified. Between $\sim$59.9°N and $\sim$62.7°N (left-most white-coloured ellipse) a tropospheric ash cloud is detected in the AIRS data and the CALIOP backscatter signal suggests these cloud layers have heights of $\sim$1–6 km. Between $\sim$68.6°N and $\sim$72.0°N (right-most white-coloured ellipse) a stratospheric cloud layer of SO$_2$ is detected in the AIRS data. The CALIOP instrument is insensitive to SO$_2$ but does scatter light from ash and SO$_2$$^{4-}$ aerosols as well as

5

Atmospheric
Chemistry
and Physics
Discussions

Open Access

EGU

meteorological clouds of ice and water droplets. The height of this layer in the CALIOP curtain is between 10–12 km and above the tropopause. The lower-right panels show vertical profiles of the backscatter for these two layer, averaged over the two latitude sections identified. These data suggest that the upper layer is most likely to be an SO_4^{2-} layer coincident with the SO_2 gas. Low volume-depolarization ratios ($\delta_v \sim 0.1$–0.2), indicative of spherical particles, within the stratospheric layer

5 are also consistent with a SO_4^{2-} layer rather than ash or ice clouds. The colour ratios (χ'; see https://eosweb.larc.nasa.gov/ PRODOCS/calipso/Quality_Summaries/CALIOP_L2LayerProducts_3.01.html for more details of these parameters) are $\chi' \sim 1$ for ash and $\chi' \sim 0.5$ for SO_4^{2-}, showing a clear difference between these two aerosol layers. The ash layer shows considerable vertical structure, with thin layering evident below 3 km and a broader feature peaking ~ 4.5 km. These data provide compelling evidence for ash and SO_2 (and SO_4^{2-}) separation from the Grímsvötn eruption, and also provide quantitative estimates of the

10 height separation with a lower troposphere ash cloud and a stratospheric gas and aerosol cloud.

4.3 SO$_2$ gas

The satellite instruments used to retrieve SO_2 are also shown in Table 1. Details of the retrieval algorithms may be found in the papers by Prata and Bernardo (2007) for the Atmospheric Infrared Sounder (AIRS), by Yang et al. (2007) for the Ozone Monitoring Instrument (OMI) and Clarisse et al. (2008) for IASI. AIRS data provides an excellent view of the SO_2 dispersion;

15 see the Supplemnatry figure S2. SO_2 was first detected in AIRS data at 03:35 UTC on 22 May, which was the first overpass of the Aqua satellite platform over Iceland following the initial Grímsvötn eruption. A large cloud of SO_2 gas was detected over the Vatnajökull glacier, slighly displaced to the north of Grímsvötn. In subsequent AIRS overpasses the SO_2 cloud grew larger and spread predominantly northwards, reaching the Greenland coast by 04:17 UTC on 23 May, ~ 12 hours later. The SO_2 cloud then spread westwards and eastwards while still propagating northwards into a long filament. The SO_2 layer height cannot be

20 inferred directly from the AIRS retrievals, but the direction of travel and transport modelling suggests a height of ~ 8–10 km; which implies the SO_2 was stratospheric. The mass of upper troposphere lower stratosphere (UTLS) SO_2 calculated from the AIRS data is shown in Figure 6. The maximum SO_2 mass was found to be $\sim 0.24 \pm 0.05$ Tg at 14:00 UTC on 23 May, 2011. Although the AIRS retrievals are only strictly valid for the UTLS, in this case it is most likely that the majority ($> 90\%$) of the SO_2 was located in the UTLS. Identification of a volcanic layer in Caliop lidar data was difficult initially, suggesting that

25 conversion to SO_4^{2-} aerosol was not yet sufficient to provide a good signal and that few ash particles were collocated with the SO_2.[2] At least three other satellite sensors detected the high level SO_2 cloud: OMI on the Aura platform, GOME-2 on MetOp-A and IASI also on MetOp-A. Table 2 shows estimates of the daily SO_2 mass from each of the sensors. OMI observations are show in the Supplementary figure S3.

Although there is some disparity between the estimates from the different sensors, when the effects of differences in height

30 sensitivity, timing differences, field-of-view sizes and swath overlap are taken into account, the values fall within the expected error bounds. The means and standard deviations for 22, 23, 24, 25 and 26 May are, 0.128 ± 0.08 Tg, 0.238 ± 0.09 Tg, 0.200 ± 0.08 Tg, 0.183 ± 0.07 Tg, and 0.180 ± 0.06 Tg, respectively. We therefore conclude that between 0.13–0.24 ± 0.1 Tg SO_2

---

[2]The Caliop lidar is insensitive to SO_2 gas, but backscatter depolarisation and colour ratio values from both SO_4^{2-} and ash particles can often be identified for strong layers.
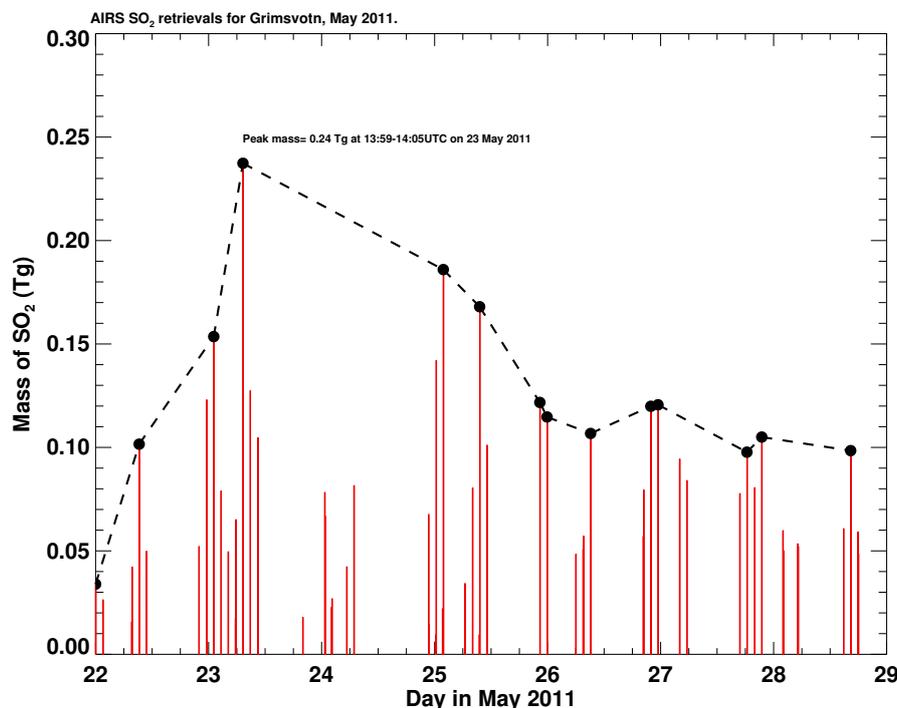
Atmospheric
Chemistry
and Physics
Discussions

Figure 6. AIRS UTLS SO_2 mass loading (Tg) as a function of time for 22–29 May, 2011. The dashed line shows the locus of maximum mass loadings – since AIRS sometimes has incomplete coverage of the whole plume a true estimate of the maximum SO_2 mass is difficult.

was released into the UTLS by Grímsvötn during the period 22–26 May, 2011. Carn *et al.* (2016) estimated a maximum SO_2 loading of 0.38 Tg.

Table 2. SO_2 total mass estimates from four different satellite instruments (two infrared and two ultraviolet) from 22–26 May 2011. [1]L. Clarisse, private comm. [2]A. Richter, http://www.iup.uni-bremen.de/scia-arc/

Instrument	Date in May, 2011				
	22	23	24	25	26
	Total mass (Tg)				
AIRS	0.10	0.24	0.18	0.12	0.11
IASI[1]	0.23	0.32			
OMI	0.15	0.28	0.29	0.25	0.20
GOME-2[2]	0.03	0.11	0.13	0.18	0.23

Atmospheric
Chemistry
and Physics
Discussions

Open Access

4.4 Ash

Volcanic ash retrievals were performed using the methods outlined by Wen and Rose (1994) and Prata and Prata (2012). Data from MODIS, AIRS and IASI, all on polar-orbiting platforms were used to determine brightness temperatures and ultimately fine (effective radii < 16 μm) ash mass loadings and particle sizes. Geostationary data from SEVIRI provided measurements

5 every 15 minutes from which brightness temperatures in 5 infrared channels could be used to detect and quantify the fine ash component. Figure S4 (supplementary) shows ash mass and effective particle size retrievals from SEVIRI at 6 hourly intervals on 23 May 2011.

The mass of fine ash was estimated using SEVIRI images by averaging in hourly intervals (4 estimates per hour) and adjusting the estimates for changes in viewing angle, which cause an error in the cloud top temperature estimation. For this

10 case, the zenith viewing angle decreased from $\sim 60°$ to $\sim 10°$ as the ash cloud progressed eastwards. Mass estimates increased by ~ 0.05 Tg.

The maximum mass of fine ash was estimated to be 0.19 ± 0.03 Tg late on 23 May. Four MODIS overpasses were also used to estimate fine ash mass, shown in Fig. 7 together with estimates from IASI (Clarisse, private communication; also see Moxnes et al. (2014)) that are sampled twice per day. The MODIS retrievals are shown in Figure S4 (supplementary material).
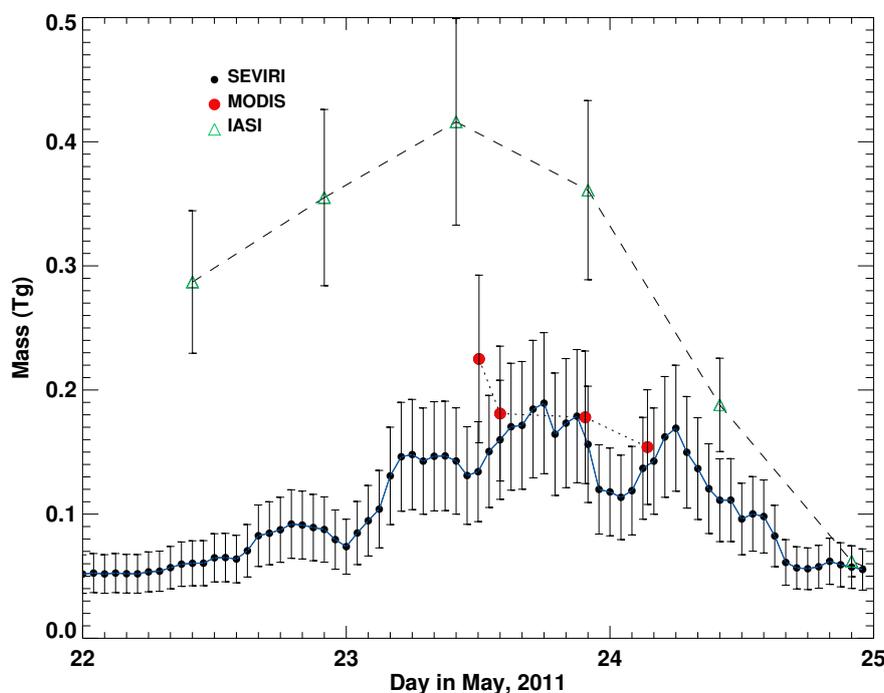

Figure 7. Fine ash mass (Tg) estimated from SEVIRI, MODIS and IASI data for the period 22–24 May, 2011.

The MODIS data give slightly higher estimates than SEVIRI, decreasing from ∼0.23 Tg at 12:05 UTC on 23 May to ∼0.15 Tg at 03:25 UTC on 24 May. The low SEVIRI estimates at the start of the series are a consequence of the inability of the SEVIRI retrieval scheme to quantify ash at these high zenith viewing angles and the confounding effects of meteorological cloud that sometimes overlaid the ash (the ash layer was mostly confined to heights below ∼ 3 km; see also Fig. 8). IASI
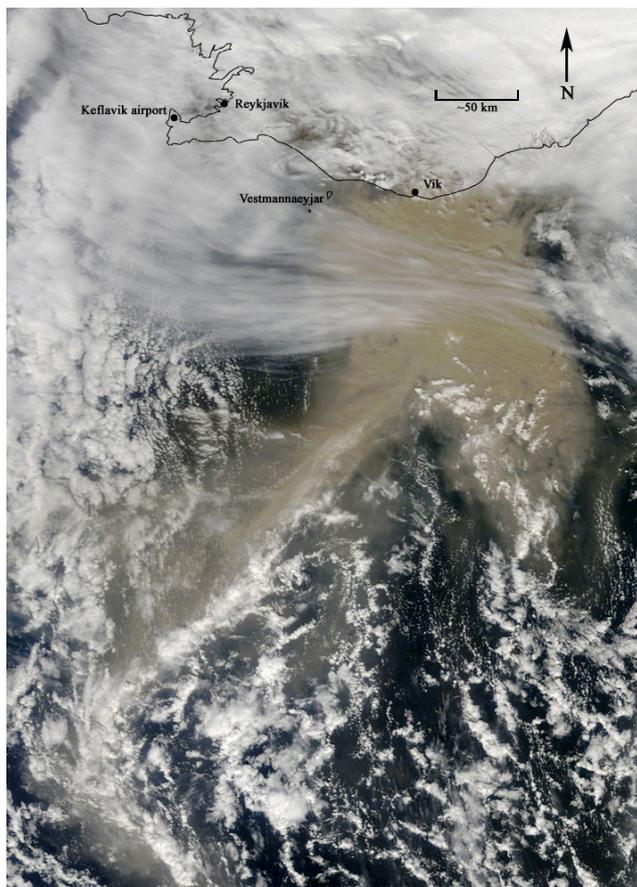

Figure 8. MODIS true-color image showing the low-level ash cloud coming off Iceland and spreading southwards. Notice that meteorological cloud is clearly evident above the ash layer and is either obscuring the ash layer over Iceland, or the ash layer ends near the coast. Grímsvötn is just off the image to the north. (*Image: MODIS/Terra, 23 May 2011, 12:05 UTC.*)

retrievals are consistently higher than SEVIRI and MODIS until late on 24 May when there is closer agreement. Prata and Prata (2012) showed that the SEVIRI mass loading retrievals were consistent with ground level PM10 concentration measurements at several stations in Scandanavia (e.g. at Bergen and Oslo), if the ash cloud was assumed to be confined to a layer no deeper than 3 km. The reason for the large differences between IASI and SEVIRI retrievals is under investigation, but IASI has a greater sensitivity to ash due to the higher spectral resolution, and the assumptions used in the retrievals are different. It is

also clear from some of the MODIS images that meteorological cloud overlaid the ash cloud and it is difficult to retrieve ash from these broadband low spectral resolution data under these circumstances. The error in estimating fine ash mass from infrared retrievals has been investigated by Wen and Rose (1994) and Prata and Prata (2012), who suggest errors of 40–50%. We estimate that the amount of ash transported towards Europe between 22–25 May, 2011 was 0.2–0.4±0.1 Tg (fine ash). By

5 comparison, Stohl et al. (2011) estimated 8.3±4.2 Tg of fine ash emitted during the Eyjafjallajökull eruption in April–May, 2010, which is an order of magnitude greater from an eruption that was an order of magnitude smaller in total erupted mass than the Grímsvötn eruption.

5   Separation of the dispersing volcanic cloud

The observational evidence for significant separation of ash and SO_2 is unequivocal, but was this entirely due to wind shear?

10 Certainly at some stages during the eruption the column reached at least 16 km and wind data show that wind shear was present, which suggests the emissions would disperse in different directions. During the period between the early morning of 22 May and late afternoon of 23 May, satellite, radar and photographic evidence shows that the column was changing height and at times extending to less than 10 km. AIRS near real-time brightness temperatures can be used to retrieve upper level SO_2 in the atmosphere. A series of six images of this product are shown in Figure S2. These products are based on brightness

15 temperatures at specific wavenumbers that correspond to SO_2 absorption locations and a radiative transfer model is used to fit the spectral features to the SO_2 column amount. A more simplified product is also used, indicating SO_2 as negative temperature differences, where $\Delta T < -6K$. Positive differences found in these images are due to other causes and strongly positive values are generally unusual. Figure 9 shows three of these brightness temperature difference products.

    The SO_2 feature is clearly evident in these images, but there is also a positive difference coincident with the location of the

20 Grímsvötn vent. We speculate that the positive temperature differences correspond to the location of the ash-rich eruption column, slightly displaced from the upper level dispersing SO_2. Interestingly, by 04:17 UTC on 23 May 2011 this positive anomaly has disappeared. The brightness temperature difference is determined from two channels at 1361.44 cm^{-1} and 1433.06 cm^{-1} situated inside and outside of the strong ν_3 SO_2 absorption band (Prata and Bernardo, 2007). The reason for the positive difference over the column is unclear, but we suggest that because these two channels are sounding the atmosphere with peak

25 contributions at different heights, a positive difference will be observed when the top of the column is below the upper level sounding channel (1433.06 cm^{-1}) peak, and above or near to the weighting function peak of the lower level channel (1361.44 cm^{-1}). This interesting observation suggests that it may be possible to utilise the AIRS spectral information to determine ash column heights for opaque columns. The changes in height of the ash column and vertical emplacement of ash is a significant process that affects the subsequent direction of transport of volcanic ash.
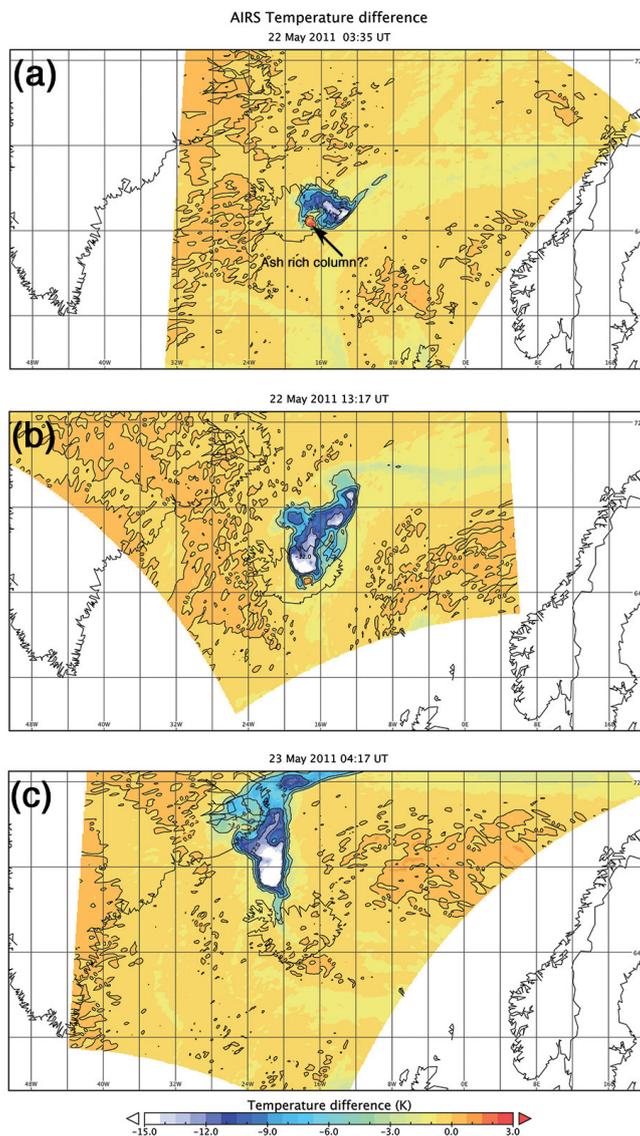
Figure 9. AIRS brightness temperature difference images for overpasses on 22 and 23 May 2011. (a) 03:35 UT, 22 May. (b) 13:17 UT, 22 May. (c) 04:17 UT, 23 May. Negative values suggest absorption by SO_2 gas. The red coloured spot (positive temperature differences) seen on panels (a) and (b) situated near the Grímsvötn vent may be due to the ash-rich column.

6 Column collapse

The MODIS satellite data shows that a low-level ash layer (<6 km high), was present off the south coast of Iceland on the morning of 22 May and is also clearly observed 24 hours later (see Fig. 8). This layer appears to be detached from the main eruption column. Photographic evidence (see Fig. 1, lower panel) shows a shallow ash cloud/plume[3] at low level surrounding the main column, and another plume-like ash-rich layer higher up and at about half the height of the column. These observations suggest the possibility that the column may have undergone partial collapse causing an outflow of ash, not dissimilar to the outflow often observed from a collapsing thunderstorm. As large ash aggregates fall through the column, enhanced by the presence of copious amounts of water, for example see Telling et al. (2013b) for a discussion of this process, ice would have formed on the ash, increasing the size and fall speed and effectively removing particles from the column. These ice-coated ash aggregates, sometimes termed volcanic hail would have fallen out of the cloud very rapidly. The process of ash falling through the column would have caused compression of the lower part of the column, and a mechanism for driving a gravity current of ash outwards from the column. The light, easterly winds in the lower troposphere favour propagation of the outflow towards the west, as observed, but it is likely that the ash formed a 'skirt' surrounding the collapsing column. Column collapses can also cause pyroclastic flows (PF), but there does not seem to be evidence of a PF in the Grímsvötn deposit. A schematic of the proposed process is shown in Fig. 10. The outflow from this mechanism may have been relatively fast; the AIRS satellite
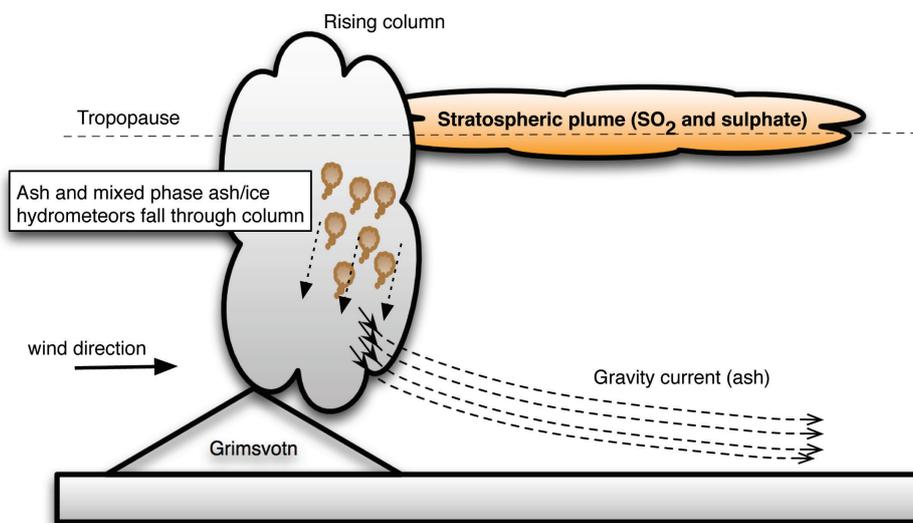

Figure 10. A schematic of the principle features of the Grímsvötn eruption column. Large hydrometeors composed of ash aggregates and mixed phase ash/ice particles fall through the column competing with the upward force of the eruption, eventually causing the column to collapse and pushing an outflow of ash-rich air into the lower troposphere. A high level plume of SO_2 and ash is capped by the tropopause.

[3]We define an ash cloud as an identifiable structure wholly disconnected from the vent, whereas an ash plume has an identifiable connection to the source vent.

observations suggest the column had stopped rising by 04:17 UTC on 23 May. The low-level ash layer persisted close to the south coast of Iceland for at least 24 hours before starting its journey further southwards and then eastwards.

The ash transported southwards from Grímsvötn which begins on 23 May arises not directly from the emissions at the vent but most likely from the collapse of the eruption column which can no longer be sustained. The southward movement of the ash can best be seen in the MODIS image acquired on 23 May 2011 at 12:05 UTC (Figure 8). The ash mass retrievals for this image (and three later images) are shown in Figure S4 (Supplementary Material) (top-left panel) where three mass loading levels are indicated: 0.2, 2 and 4 g m^{-2}.

Further support for rapid removal of ash before transport is provided in the photograph shown in Figure 11 taken on 31 May, just 8 days later on the Vatnajökull glacier near Grímsvötn. The photograph shows a short vertical section dug into the deposit with evidence of hail. The presence of hail within the deposit has also been described by Arason et al. (2011), who found hailstones of 1–2 mm size infused with ash. Gudmundsson (2013) has estimated the amount of water melted by the eruption and since no Jökulhups were observed it may be assumed that much of that water went into the plume, providing extra energy and also contributing to ice and hail formation within the column. A large amount of lightning was observed in the eruption column and clouds, also suggesting the presence of hydrometeors. It is difficult to estimate whether the column collapsed more

Figure 11. Photograph of a vertical section taken on the Vatnajökull glacier at a location where there was significant ash fall from Grímsvötn, on 31 May 2011. There is evidence of millimetre-sized hail in the deposit.

than once but there does seem to be evidence that an ash surge occurred on the morning of 22 May. A MODIS image acquired at 05:15 UTC on 22 May (∼10 hours after the start of the eruption) appears to show gravity waves emanating from the column, and a skirt of ash spreading southwards and then curving around the north-eastern coast of Iceland. These could have been formed when the column sloughed, causing a cold ash surge driven by the buoyancy force due to the vertical gradient in the density. Figure 12(a) shows the 250 m resolution MODIS band 2 (841–876 nm) image reprojected, calibrated to reflectance and digitally enhanced to highlight various features.
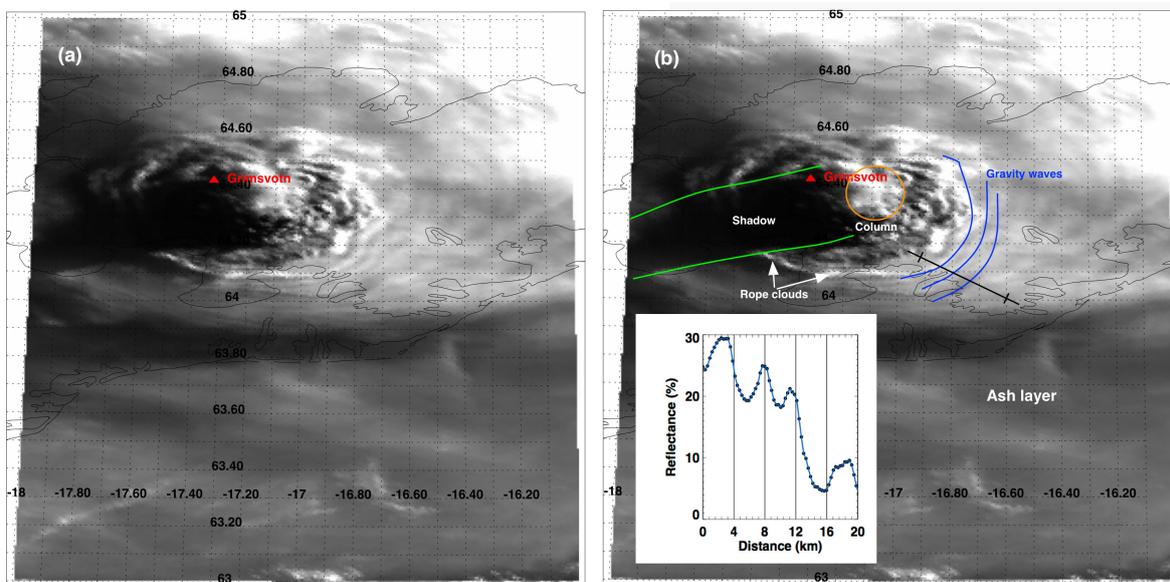
Figure 12. (a) MODIS/Aqua 250 m resolution 841–876 nm reflectance image showing the Grímsvötn ash column, ash column shadow, ash layer, rope clouds and gravity wave features. (b) Annotated version of (a) with inset plot showing reflectance along the a line (indicated in black) from the ash column towards the south-east. The blue-coloured arcs indicate the locations of wave-like fronts, the orange-coloured circle indicates the outline of the ash column, which is casting a strong shadow (westwards of the column) on the underlying clouds of ash and water clouds. The apparent wavelength of the waves is ∼4–6 km. The solar zenith and azimuth and MODIS viewing zenith and azimuth angles close to the column are: 82.5°, 56.4°, 55.5° and –53.4°, respectively. Image acquired at 05:15 UTC on 22 May 2011.

The features are identified as the Grímsvötn eruption column (slightly east of the volcano location, indicated by the red triangle), its shadow cast westwards onto a lower layer of ash and meteorological cloud, an ash layer extending along the south coast of Iceland, rope clouds, and gravity waves (Fig. 12b). The reflectance (in %) along a transect indicated by the black line is also shown inset in Fig. 12(b). Variations in reflectance along the transect occur due to height variations in the cloud and the solar/sensor viewing geometry. The approximate wavelength of the waves is ∼4–6 km. measurements reported by Petersen et al. (2012) from radars situated at Keflavik and on a mobile platform show an oscillatory behaviour of the plume top on 21–22 May with a considerable drop in height to 10 km around 20:00 UTC on 22 May, followed by a drop to 6 km (or lower) at ∼11:00 UTC on 23 May, and another drop to less than 3 km at ∼16:00 UTC. The height does not exceed 8 km thereafter.

7 Insights on the mechanisms and conditions for ash separation from a plume

The observations provide strong evidence that separation of ash occurred predominantly in the convectively-rising part of the eruption column, where the motion is driven by a buoyancy force arising from a density difference between the column and the atmosphere, rather than at the source or in the laterally intruding ash cloud. The buoyant volcanic plume is a complex

physical environment, with multiple interacting phases, highly turbulent flow fields, and coupled nonlinear physical and chemical processes occurring. Despite this complexity, much insight into the dynamics of volcanic plumes has been gained from mathematical models of turbulent buoyant plumes (Morton et al., 1956) which have been extended to model thermodynamics and transport of solids in volcanic plumes (see e.g. Wilson et al., 1978; Sparks, 1986; Woods, 1988; Glaze and Baloga, 1996;

5   Sparks et al., 1997a; Bursik, 2001; Woodhouse et al., 2013a).

Here we use an integral model of volcanic plumes to gain insight into the physical processes that could lead to an abrupt separation of ash from the plume at Grímsvötn. We adopt the integral model of Woodhouse et al. (2013a) which includes descriptions of the thermodynamics of phase changes of water, the effect of atmospheric winds on the plume dynamics, and detailed profiles of the atmospheric structure during the eruption. Additional details of our modelling approach are given in the

10   Appendix and a derivation of the system of equations adopted in our model are given in §2 and §3 of Woodhouse et al. (2013a).

Our hypothesis is that the separation of ash from the convectively-rising plume that was observed at high altitude was due to rapid aggregation of ash particles, mediated by a rapid condensation of water in the plume. The presence of (liquid) water is likely to promote the aggregation of ash particles by allowing the formation of liquid bridges between grains (Brown et al., 2012; Van Eaton et al., 2012). The capillary forces in the liquid connections are much stronger than electrostatic attractions

15   between dry grains (James et al., 2003), and therefore it is possible that wet aggregates can endure a collision which would cause dry aggregates to break apart. Aggregation in the presence of liquid water or ice is extremely efficient, with aggregation time scales less than one-tenth of a second (Veitch and Woods, 2001; Costa et al., 2010). Costa et al. (2010) demonstrate that a particle size distribution that initially has a peak number density at $10\,\mu$m can evolve to a produce a peak in the number density at $100\,\mu$m in 60 seconds in an environment with condensed water available.

20   Rather than modelling aggregation explicitly, which is subject to great uncertainty, here we use a model of volcanic plumes to investigate whether conditions in the plume are favourable for wet aggregation and an abrupt fallout of solids. The maximum elevation of solid particles of a given size can be estimated by balancing the average vertical velocity of gaseous phases in the plume with the settling-speed of a particle (see the appendix). This provides a simple, yet robust, method of examining the consequence of aggregation; the estimated maximum fallout height is determined only by the particle size and the evolution of

25   the particle size distribution is not required. Figure 13 illustrates a typical prediction obtained from our model for the plume from Grímsvötn at 05:00 UTC on 22 May 2011.

Gentle winds and the large mass flux of erupted material result in a sub-vertical plume that is little affected by the wind. The model identifies an abrupt transition in the plume from dry conditions at lower levels (below approximately $10\,$km) to an environment with a substantial amount of condensed water, and the low atmospheric temperature results in a predominance of

30   ice with peak concentration in excess of $4\,$g kg^{-1} (Fig. 13b). The critical fall-out velocity of $50\,\mu$m particles is reached at an altitude of $18\,$km asl (Fig. 13c), above the neutral buoyancy height (Fig. 13d) and so these small particles could be carried to the plume top and into the lateral intrusion. Similarly, $100\,\mu$m particles could be transported to $17\,$km asl. However, if these fine particles aggregate during their transport to produce larger grains, the velocity in the upper plume could be insufficient to support them. The velocity of the plume in the region above the condensation level falls below 5 m s^{-1} and therefore fine

35   particles will take several minutes to reach the plume top; ample time for aggregation to occur (Veitch and Woods, 2001; Costa

Atmospheric
Chemistry
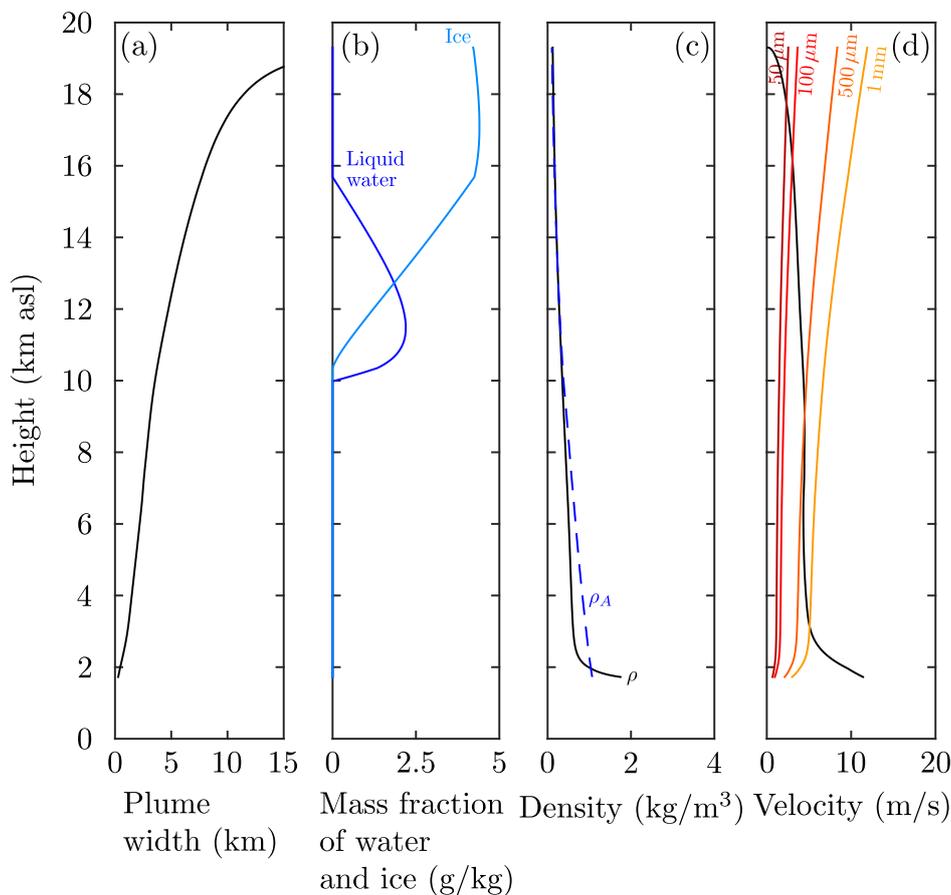and Physics
Discussions

Open Access

EGU

Figure 13. Model prediction of the Grímsvötn plume at 0500 on 22 May 2011, assuming 10wt% of water vapour at the source. (a) Plume width (taken as twice the Gaussian half-width from the plume centreline) as a function of height. (b) Mass fraction of liquid water and ice as functions of height. (c) Density of the plume ρ_P and atmosphere ρ_A as functions of height. (d) Vertical velocity of the plume at the nominal plume edge (taken as twice the Gaussian half-width from the plume centreline) and critical fall-out velocities of $50\,\mu\mathrm{m}$, $100\,\mu\mathrm{m}$, $500\,\mu\mathrm{m}$ and $1\,\mathrm{mm}$ particles as functions of height.

et al., 2010). For particles of diameters $500\,\mu m$ and $1\,mm$ the critical fall-out velocity is reached at altitudes of $11\,km\,asl$ and $6.8\,km\,asl$ respectively (Fig. 13c), which is below the neutral buoyancy height.

The small diameter grains carried above the condensation height are transported further (circulating in turbulent eddies) in an environment conducive to rapid wet aggregation, and therefore we expect the particle diameter to increase substantially. If aggregates grow sufficiently rapidly they will fall out before reaching the neutral buoyancy height. Deposits of tephra on the Vatnajökull glacier show evidence of hailstones infused with ash with diameters as large as 1–$2\,mm$. Aggregates of this size would readily fall from the plume and would be unlikely to be re-entrained into the plume due to their size and the width of the plume at the height at which fall out occurs. Smaller aggregates will also fall out of the plume but may not reach the ground proximal to the eruption column, instead being transported laterally by the wind.

8   Conclusions

The separation of material in vigorous volcanic eruptions seems inevitable in the presence of wind shear. Wind shear is ubiquitous and significant when eruption columns extend to the tropopause and consequently it should always be expected that separation will occur. Since also gases and particles are not always released in unison, the time-varying nature of the wind fields might also lead to separation even for a steady, low level eruption column. Gases and particles also separate within the column due to aggregation of particles and the formation of mixed phase particles of ice and ash that can lead to rapid fall-out, leaving lighter gases at higher levels in the column. These interactions between the erupting volcanic column and the atmospheric environment in the vicinity of the volcano are important for the short- and long-range transport of gas and particles.

A combination of satellite observations (passive and active) and dispersion modelling has been used to study the separation of ash and SO_2 and it is apparent that such data could be readily utilised in dispersion models by using assimilation (Fu et al., 2017) or through the use of inversion techniques (Stohl et al., 2011). Whether these techniques are sufficiently sensitive to predict separation or perhaps more importantly column collapse, remains to be investigated. The model used here that treats the dispersing ash as a buoyant plume successfully reproduces some of the salient features found in the observations and demonstrates the importance of water in vigorous erupting volcanic columns. Clearly more detailed and complex modelling is needed and we recommend that future studies using VATDs consider gases and particles separately and improve parametrisations of the physics of erupting columns. Separation of gases and particles in volcanic eruptions occurs frequently and it seems logical to treat, at least much of the time, the sources separately. Column collapse is not an exceptional event and suggests that this process should be included as a mechanism for ash generation and subsequent transport in VATDs. The overwhelming observational evidence for maximum separation with high-level SO_2 travelling northwards and low-level ash travelling southwards led to a re-evaluation of model forecasts during the Grímsvötn event, which initially forecast ash collocated with high-level SO_2 and covering a large geographic region extending northwards and eastwards from Iceland towards Greenland and the western Norwegian coast (see Fig. 14).
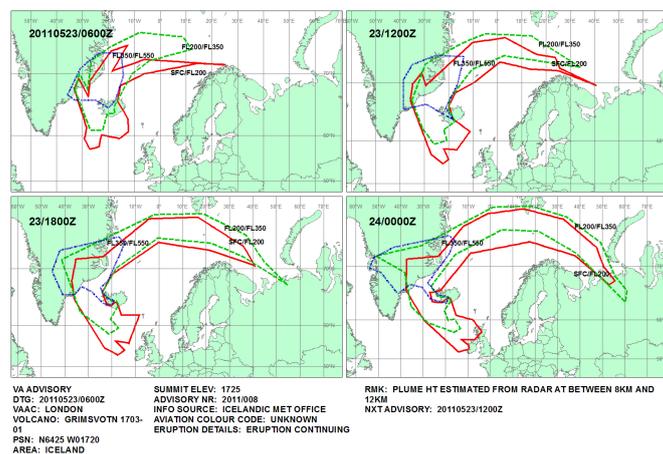
Figure 14. Volcanic ash graphic (VAG) issued by the London VAAC on 23 May 2011 at 06:00 UTC. The forecast is valid for the following 18 hours, in 6 hour intervals and shows forecast ash regions from the surface to two flight levels: FL200 (20,000 ft in red) and FL350 (35,000 ft, in green dashes).

The volcanic ash advisory also shows a region of potentially highly concentrated ash apparently extending to FL200 (20,000 ft or 7 km) travelling southwards and extending eastwards towards Scotland. This erroneous forecast led to closure of airspace over parts of northern Europe and disruption of some air traffic. In the event, observed concentrations did not exceed 2 mg m^{-3} on arrival over northern Europe, and were mostly less than 1 mg m^{-3}, suggesting that the ash layer was not sufficiently concentrated to be a hazard to aircraft; although we caution that without agreed engine manufacturers' tolerance limits the actual dangerous ash concentration (or dosage) is unknown.

Observational data of the kind presented here can be used to constrain VATD models (Stohl et al., 2011) and such models should treat at least the gas and particle components separately. A straightforward way to do this is to extend the methods proposed by Eckhardt et al. (2008), Kristiansen et al. (2010) and Stohl et al. (2011) to include two sources. Improvements in dealing with the complex nature of the interaction of the atmosphere with the erupting column are needed: including better parameterisations of the aggregation process (e.g. Textor et al., 2006; Costa et al., 2010; Telling et al., 2013b), improved understanding of bent-over plumes (Woodhouse et al., 2013b), and improved modelling of the effects of partial or total column collapse. While perhaps less common, except in large eruptions (VEI>4), column collapse can lead to the generation of pyroclastic flows that can act as secondary sources for new column generation, so-called co-ignimbrite plumes (Self and Rampino, 1981). These can be vertically extensive (several kilometres), ash-rich and hence significant in forecasting transport of the aviation hazard. It is suggested here that one or more partial column collapses at Grímsvötn led to surges of 'cold' ash layers that eventually led to transport of ash towards Scotland and southern Scandanavia. This source mechanism is not currently included in ash dispersion models. During the Grímsvötn event the London VAAC used the state-of-the-science dispersion model, NAME (Jones et al., 2007) driven by a source term that relates the total mass erupted to the fourth power

of the column height. The fine mass fraction is taken as a small percentage of the total mass; 5% is often used. Clearly, if the column collapses then this parametrisation of the source term is not appropriate.

Emissions of gases and particles into the atmosphere from Icelandic volcanoes can have important consequences for the local environment and also for Europe (Thordarson and Self, 2003). The mechanisms and processes controlling the behaviour of eruptions are vital to understand. Both near-field processes (e.g. ash and gas generation, column collapse, wind structure, aggregation and fall-out) and far-field processes (dispersion, wet/dry deposition, chemical conversion, and aggregation) are important and it is likely that with constraints on these processes better forecasts of the movement of the erupted products can be made.

The transport and fate of SO_2 in the atmosphere has implications for the atmospheric radiative balance. Eruptions that generate large amounts of SO_2 able to penetrate the tropopause can lead to global surface cooling (Robock, 2000) and hence it is important to know the vertical emplacement of SO_2 from such eruptions. Approximately ~ 0.13–0.24 ± 0.1 Tg of SO_2 was released by the 21-28 May 2011 eruption of Grímsvötn; nearly all of which resided above the tropopause. The e-folding time for conversion of SO_2 to SO_4^{2-} aerosol in the stratosphere is on the order of 20–30 days (Guo et al., 2004), making transport processes likely to cause hemispheric spread of the aerosol. In the case of this Grímsvötn eruption, the amount of SO_2 released was too small to have a noticeable climate impact. Approximately 0.2–0.4$\pm$0.1 Tg of fine ash was also released, again too small to have an appreciable effect on the radiative balance, and not significant enough to cause a hazard to aviation.

Atmospheric
Chemistry
and Physics
Discussions

Appendix: Appendix: Modelling volcanic plumes, aggregation and particle support

Model description

Plume models have been used extensively to examine the dynamics of volcanic eruption columns (Sparks et al., 1997a). While
there have been attempts to explicitly model aggregation in plumes (see e.g. Veitch and Woods, 2001; Costa et al., 2010), the
5   models are sensitive to empirical parameters that are not well constrained. Indeed, the physical characteristics (e.g. shape, size,
porosity etc.) and chemical composition of volcanic ash particles are likely to greatly alter the aggregation efficiency (James
et al., 2002; Durant et al., 2009; Brown et al., 2012; Telling et al., 2013a) and these properties vary substantially for different
eruptions. Furthermore, in describing the evolution of aggregating particles, knowledge of the initial particle size distribution
is required. The uncertainty introduced by incomplete models, parameters calibrated on small data sets, and unknown initial
10   conditions means that current models of aggregation are unlikely to produce robust predictions for specific events. We instead
examine the changing conditions within the plume and assess the effect this could have on the transport of ash particles. This
approach does not couple the evolving particle size distribution to the plume dynamics. However, it provides insight into the
possibility of rapid aggregation with an abrupt onset.

The plume model of Woodhouse et al. (2013a) calculates profiles of plume properties (such as the plume radius, axial
15   velocity, temperature, and the mass fractions of magmatic and atmospheric gases and liquid water) along the plume trajectory,
which may be bent-over by the atmospheric wind field. For the Grímsvötn eruption, the wind speeds were not sufficient to
significantly affect the plume during its ascent, which was almost vertical. For vertically rising plumes, analogue laboratory
experiments (Morton et al., 1956; Papanicolaou and List, 1988) show that the radial profiles of (time-averaged) axial velocity
and density deficit are well-described by Gaussian functions. The action of eddies at the margins of the highly turbulent flow in
20   the plume results in entrainment of atmospheric air, which reduces the density difference and eventually (in a stably stratified
ambient) the plume reaches the neutral buoyancy height (where the density of the plume equals the atmospheric density) and
the plume begins to intrude laterally into the atmosphere (Sparks et al., 1997a; Bursik, 1998; Johnson et al., 2015).

The ash particles transported upwards in the plume are supported by the gaseous phases which exert a drag on the grains
sufficient to overcome their weight. Particles can fall out of the plume if they are transported to regions where the gas velocity
25   is not sufficient to support the weight of the grains, which can occur at the plume margins (due to the radial Gaussian profile
of vertical velocity) or at a sufficient altitude as the plume decelerates, although fine particle fractions can also be transported
into the horizontally intruding layer and subsequently carried to great distances.

The transport and change of phase of water in the plume can play an important role in the plume dynamics (Woods, 1993;
Glaze and Baloga, 1996; Woodhouse et al., 2013a). Water vapour exsolved from magma or incorporated from surface water
30   or ice around the vent, in addition to water vapour entrained from the moist troposphere, can be carried to high altitude in the
relatively hot plume. Cooling of the plume due to entrainment and the reduction in pressure during ascent can result in the
plume becoming saturated with respect to water vapour, at which point the water vapour condenses, aided by the presence of
condensation nuclei in the form of fine ash particles (Woods, 1993). The release of latent heat of condensation can lead to a
substantial increase in the rise height of the plume in comparison to a dry eruption column that does not become saturated.

Atmospheric
Chemistry
and Physics
Discussions

This process is particularly important in the moist tropics (Tupper et al., 2009) but can also occur at high latitudes (Woodhouse and Behnke, 2014; Van Eaton et al., 2015). If the plume ascends to altitudes at which the temperature falls below the water freezing temperature, water droplets may begin to freeze. We model ice formation using the approach of Mastin (2007), with a mixture of ice and super-cooled liquid water present for temperatures between $0°C$ and $-40°C$ with mass fractions linearly

5 dependent on the temperature.

To form aggregates, particles must be brought sufficiently close together that electrostatic forces of attraction can bind them or liquid films on the surfaces can coalesce. In the lower region of the plume there is a high concentration of particles, so it might be expected that aggregation occurs here rather than in the upper part of the plume, where entrainment of atmospheric air has greatly reduced the particle concentration. However, the lower part of the plume typically has higher velocities, leading

10 to greater kinetic energy of particle collisions, which reduces the efficiency of aggregation (Telling and Dufek, 2012). The presence of liquid water increases substantially the aggregation efficiency (Telling et al., 2013a) and, because condensation and freezing typically occur at high altitudes in the plume, the lower velocity of the plume reduces the kinetic energy of collisions. We therefore expect that aggregation proceeds rapidly in 'wet' conditions, resulting in a pronounced increase in the size of particle clusters, while electrostatically dominated aggregation in 'dry' regions results in more gradual growth of

15 clusters.

We consider a particle of diameter d and density ρ_s that is transported with speed u_s in the plume that is rising with vertical velocity u_p. The hydrodynamic drag acting on the particle is given by

$$F_D = \frac{\pi d^2}{8} \rho_p C_D \left(u_s - u_p\right)^2 \operatorname{sgn}\left(u_p - u_s\right),$$ (1)

where ρ_p is the bulk density of the plume and C_D is the drag coefficient of the particle. Balancing drag with the weight of the

20 particle at the point when the particle is no longer supported by the plume (i.e. $u_s = 0$), we find that

$$\frac{\pi d^2}{8} \rho_p C_D u_p^2 = \frac{\pi d^3}{6} \rho_s g$$ (2)

and therefore the particle falls out of the plume when

$$u_p \leqslant \left(\frac{4 d \rho_s g}{3 \rho_p C_D}\right)^{1/2} \equiv u_c(d),$$ (3)

where $u_c(d)$ is the critical fall-out velocity for a particle of diameter d. The value of the drag coefficient depends on properties

25 of the particle, particularly shape, and on the Reynolds number of the flow field in which it is carried (Wilson and Huang, 1979). Furthermore, the drag coefficient of aggregates may differ from that of individual particles (James et al., 2003). Here we take a representative value of $C_D = 1$ noting that $u_c(d)$ is not strongly sensitive to the value of the drag coefficient.

We assume that the radial profile of the mean axial velocity of the plume is Gaussian,

$$u_p(r,z) = u(z) \exp\left(-r^2/R^2\right),$$ (4)

30 where r is the radial distance from the centreline of the plume and R is a characteristic radial length scale. The radial distance $r = 2R$ is taken as representative of the plume width, and at that point the local mean axial velocity of the plume is less than 2% of the centreline value.

Atmospheric
Chemistry
and Physics

Open Access

Discussions

EGU

Model Results

At 05:00 UTC on 22 May 2011, the C-band weather radar at Keflavik International Airport recorded a plume height of $19.3\,\mathrm{km}$. The mass flux of erupted material is estimated by matching the model prediction of the plume height to the radar observation

5   with fixed values of the vent radius, gas mass fraction and temperature at the source (table **??**). The resulting source mass flux estimate is $Q_0 = 9.5 \times 10^7\ \mathrm{kg\ s^{-1}}$.

Table 3. Source parameter value used in the plume model for 0500 on 22 May 201.

Parameter (symbol)	Value
Vent radius (L_0)	$200\,\mathrm{m}$
Source gas mass fraction (n_0)	0.05
Source temperature (T_0)	$1000\,\mathrm{K}$
Vent altitude (z_0)	$1725\,\mathrm{m}$

Figure 15 shows time series of the plume height and condensation level, the maximum mass fractions of liquid water and ice in the plume, and the critical height at which particles fall out of the plume for four particle diameters on the 22 May 2011. Plume top heights are derived from a fixed C-band radar and a mobile X-band radar. The variation of the condensation level in

10   the plume follows that of the plume top height. The mass fractions of liquid water and ice in the plume do not vary substantially (with the exception of a decrease in the ice content at 09:00 and 10:00 UTC) despite changes in the condensation height, and there is a plentiful supply of condensed water in the plume throughout this period of the eruption. There are pronounced differences in the critical fall-out heights of particles of different diameters. Particles of diameter $50\,\mu\mathrm{m}$ are carried to near to the plume top height, above the condensation level. Often $100\,\mu\mathrm{m}$ diameter particles are carried above the condensation level,

15   but we note that between 09:00 and 10:00 UTC on 22 May the critical fall-out velocity of these particles is reached at low levels in the plume. The larger particles (diameters of $500\,\mu\mathrm{m}$ and $1\,\mathrm{mm}$) consistently fall out below the condensation level. The period between 09:00 and 10:00 UTC on 22 May is distinctive in the relatively low plume height, ice content and low critical fall-out height for particles of diameter greater than $500\,\mu\mathrm{m}$. The low plume height requires a reduced mass flux from the source and therefore relatively low velocities in the plume. Thus the critical fall-out velocity of a particle occurs at lower

20   altitudes. Therefore, during this period the fall out of relatively small diameter particles could occur without significant wet aggregation; dry aggregation in the lower plume might be sufficient to remove fine ash.

The model source conditions used above (table **??**) have a relatively dry source with a water vapour mass fraction of $5\,\mathrm{wt}\%$. However, the melting of glacier ice around the vent at Grímsvötn is likely to have contributed water vapour in addition to that derived from magma. The sensitivity of the model predictions to the source water mass fraction is examined in Figure 16

25   where the water vapour content is taken to be $5\,\mathrm{wt}\%$, $10\,\mathrm{wt}\%$ and $15\,\mathrm{wt}\%$. Adding water at the source has a pronounced effect on the condensed water content of the plume, with both the mass fractions of the condensed phases increasing and the level at which condensation occurs decreasing as the source mass fraction of water vapour increases. When the source is relatively
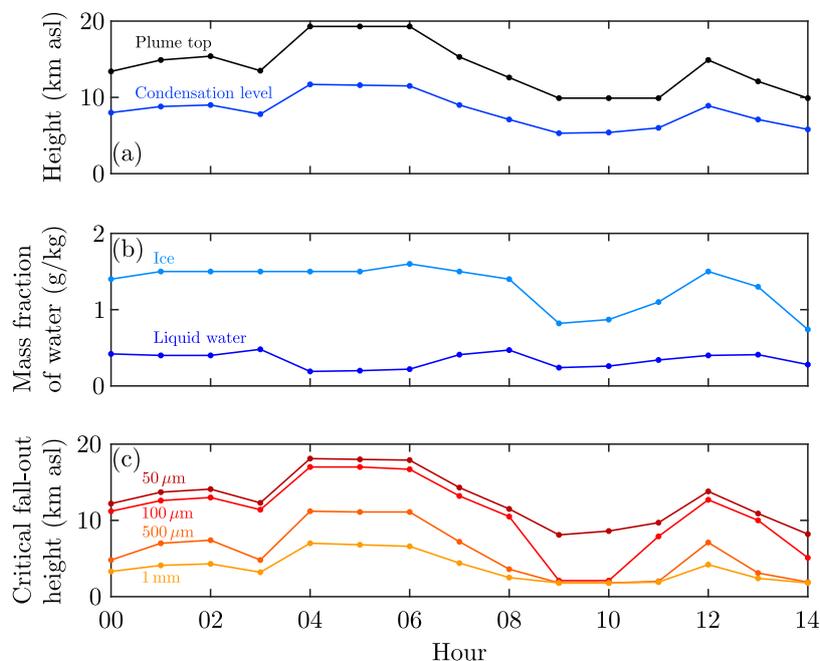
Atmospheric
Chemistry
and Physics

Discussions

Figure 15. Model predictions of the properties of the Grímsvötn plume on 22 May 2011. (a) Plume top height and condensation level in the plume. (b) Maximum mass fractions of liquid water and water ice. (c) Critical height at which particles fall-out of the plume for particles of diameters $50\,\mu$m, $100\,\mu$m, $500\,\mu$m and $1\,$mm.

dry, with $n_0 = 0.05$, condensation occurs when the plume temperature is below $0°$C, so liquid water and ice are expected to form. In contrast, for both $n_0 = 0.1$ and $n_0 = 0.15$ the condensation occurs when the plume temperature exceeds $0°$C and therefore the vapour first condenses to water, with ice forming at higher altitudes as the temperature decreases. We note that the source mass fraction of water vapour strongly influences the buoyancy of the erupted material at the source; for $n_0 = 0.05$ and $n_0 = 0.1$ the erupted material is initially more dense than the atmosphere and is driven upwards by momentum, whereas the material is buoyant at the vent when $n_0 = 0.15$. Interestingly, the velocity at the source when $n_0 = 0.15$ is greater than that when $n_0 = 0.1$. However, the dependence of the fall-out velocity on the plume density means that the fall-out height for each particle size decreases substantially as n_0 increases.

Figure 16 demonstrates that the potential for the separation of fine ash from the plume, driven by wet aggregation, increases substantially as the source water vapour content increases. However, for the atmospheric conditions at the time of the Grímsvötn eruption, the model predicts substantial concentrations of condensed water for all of the source conditions examined. Therefore, our hypothesis of water-mediated aggregation and enhanced removal of ash from the plume is robust to changes in the source conditions.
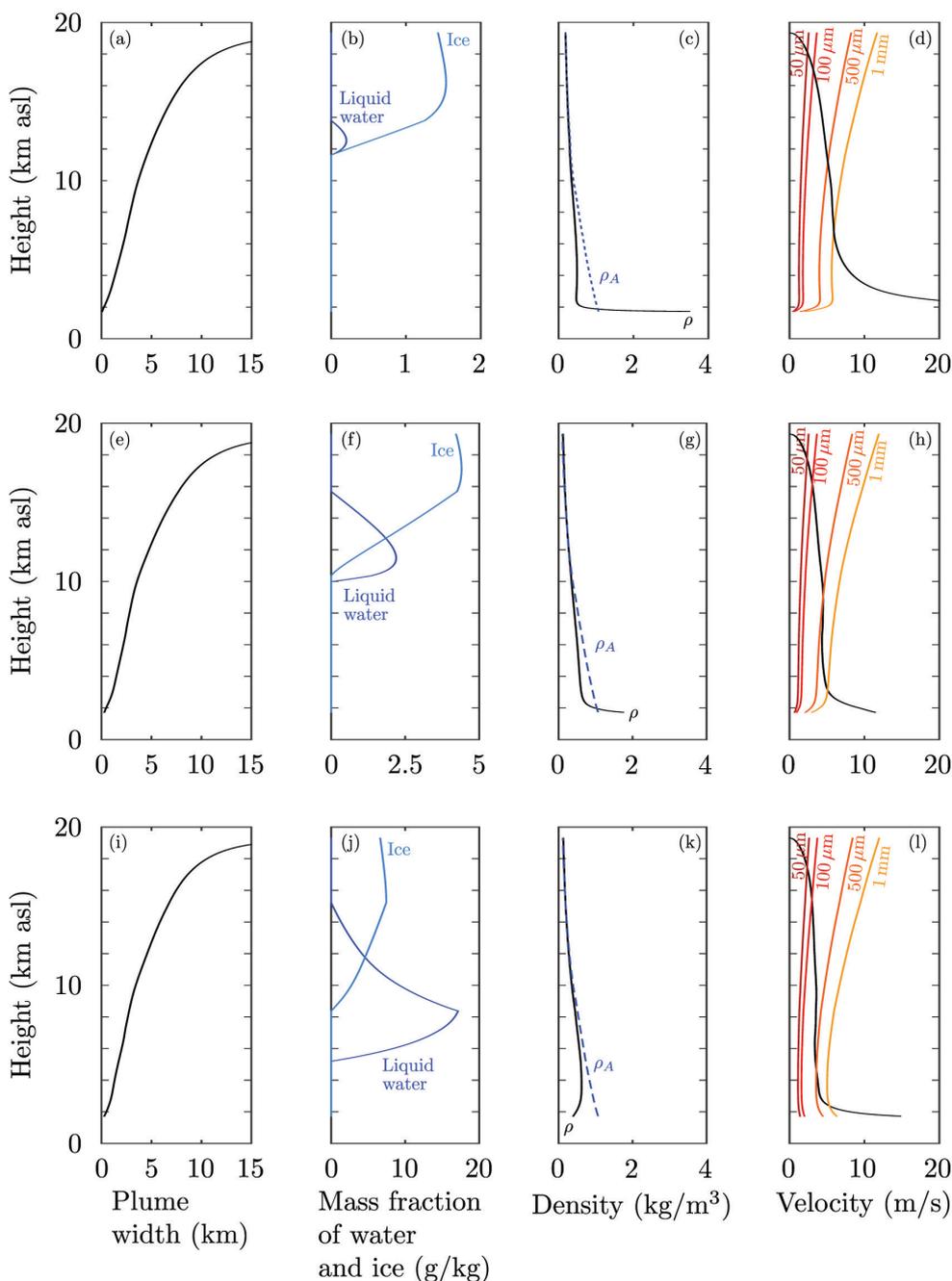
Atmospheric
Chemistry
and Physics
Discussions

Figure 16. Sensitivity of model predictions of the Grímsvötn plume at 0500 on 22 May 2011 to increases in the source water vapour content, with (a-d) $n_0 = 0.05$, (e-h) $n_0 = 0.10$ and (i-l) $n_0 = 0.15$. (a,e,i) Plume width as a function of height. (b,f,j) Mass fraction of liquid water and water ice as a function of height. (c,g,k) Density of the plume ρ_P and atmosphere ρ_A as functions of height. (d,h,l) Vertical velocity of the plume at the plume edge and critical fall-out velocities of $50\,\mu$m, $100\,\mu$m, $500\,\mu$m and $1\,$mm particles as functions of height.

Atmospheric
Chemistry
and Physics
Discussions

Open Access

EGU

References

Arason, P., Petersen, G., and Bjornsson, H.: Observations of the altitude of the volcanic plume during the eruption of Eyjafjallajökull, April–May 2010, Earth System Science Data Discussions, 4, 1–25, 2011.

5 Bourassa, A. E., Robock, A., Randel, W. J., Deshler, T., Rieger, L. A., Lloyd, N. D., Llewellyn, E. T., and Degenstein, D. A.: Large volcanic aerosol load in the stratosphere linked to Asian monsoon transport, Science, 337, 78–81, 2012.

Brown, R., Bonadonna, C., and Durant, A.: A review of volcanic ash aggregation, Physics and Chemistry of the Earth, 45–46, 65–78, doi:doi:10.1016/j.pce.2011.11.001, 2012.

Bursik, M.: Tephra dispersal, Geological Society, London, Special Publications, 145, 115–144, doi:10.1144/GSL.SP.1996.145.01.07, 1998.

10 Bursik, M.: Effect of wind on the rise height of volcanic plumes, Geophysical Research Letters, 28, 3621–3624, 2001.

Carn, S., Strow, L., de Souza-Machado, S., Edmonds, Y., and Hannon, S.: Quantifying tropospheric volcanic emissions with AIRS: The 2002 eruption of Mt. Etna (Italy), Geophysical Research Letters, 32, 2005.

Carn, S., Clarisse, L., and Prata, A.: Multi-decadal satellite measurements of global volcanic degassing, Journal of Volcanology and Geothermal Research, 2016.

15 Clarisse, L., Coheur, P.-F., Prata, A. J., Hurtmans, D., Razavi, A., Phulpin, T., Hadji-Lazaro, J., and Clerbaux, C.: Tracking and quantifying volcanic SO_2 with IASI, the September 2007 eruption at Jebel at Tair, Atmospheric chemistry and physics, 8, 7723–7734, 2008.

Clarisse, L., Prata, F., Lacour, J.-L., Hurtmans, D., Clerbaux, C., and Coheur, P.-F.: A correlation method for volcanic ash detection using hyperspectral infrared measurements, Geophysical research letters, 37, 2010.

Costa, A., Folch, A., and Macedonio, G.: A model for wet aggregation of ash particles in volcanic plumes and clouds: 1. Theoretical
20 formulation, Journal of Geophysical Research: Solid Earth (1978–2012), 115, 2010.

Draxler, R. and Rolph, G.: HYSPLIT (HYbrid Single-Particle Lagrangian Integrated Trajectory) model access via NOAA ARL READY website (http://www. arl. noaa. gov/ready/hysplit4. html). NOAA Air Resources Laboratory, Silver Spring, 2003.

Durant, A., Rose, W., Sarna-Wojcicki, A., Carey, S., and Volentik, A.: Hydrometeor-enhanced tephra sedimentation: Constraints from the 18 May 1980 eruption of Mount St. Helens, Journal of Geophysical Research, 114, B03 204, doi:10.1029/2008JB005756, 2009.

25 Eckhardt, S., Prata, A., Seibert, P., Stebel, K., and Stohl, A.: Estimation of the vertical profile of sulfur dioxide injection into the atmosphere by a volcanic eruption using satellite column measurements and inverse transport modeling, Atmospheric Chemistry and Physics, 8, 3881–3897, 2008.

Folch, A., Costa, A., and Macedonio, G.: FALL3D: A computational model for transport and deposition of volcanic ash, Computers & Geosciences, 35, 1334–1342, 2009.

30 Fromm, M., Kablick, G., Nedoluha, G., Carboni, E., Grainger, R., Campbell, J., and Lewis, J.: Correcting the record of volcanic stratospheric aerosol impact: Nabro and Sarychev Peak, Journal of Geophysical Research: Atmospheres, 119, 2014.

Fu, G., Prata, A., Lin, H., Heemink, A., Segers, A., and Lu, S.: Data assimilation for volcanic ash plumes using a satellite observational operator: a case study on the 2010 Eyjafjallajökull volcanic eruption, Atmos. Chem. Phys., 17, 1187–1205, 2017.

Glaze, L. and Baloga, S.: Sensitivity of buoyant plume heights to ambient atmospheric conditions: Implications for volcanic eruption
35 columns, Journal of Geophysical Research, 101, 1529–1540, doi:10.1029/95JD03071, 1996.

Gudmundsson, M., Höskuldsson, Á., Larsen, G., Thordarson, T., Oladottir, B., Oddsson, B., Gudnason, J., Högnadottir, T., Stevenson, J., Houghton, B., et al.: The May 2011 eruption of Grímsvötn, in: EGU General Assembly Conference Abstracts, vol. 14, p. 12119, 2012a.

Gudmundsson, M. T., Thordarson, T., Höskuldsson, Á., Larsen, G., Björnsson, H., Prata, F. J., Oddsson, B., Magnússon, E., Högnadóttir, T., Petersen, G. N., et al.: Ash generation and distribution from the April-May 2010 eruption of Eyjafjallajökull, Iceland, Scientific reports, 2, 2012b.

5 Guo, S., Bluth, G. J., Rose, W. I., Watson, I. M., and Prata, A.: Re-evaluation of SO2 release of the 15 June 1991 Pinatubo eruption using ultraviolet and infrared satellite sensors, Geochemistry, Geophysics, Geosystems, 5, 2004.

Hoffmann, L., Grießbach, S., and Meyer, C. I.: Volcanic emissions from AIRS observations: detection methods, case study, and statistical analysis, in: Proceedings of the SPIE, p. 924214, Forschungszentrum Jülich GmbH (Germany), 2014.

Holasek, R. E., Woods, A. W., and Self, S.: Experiments on gas-ash separation processes in volcanic umbrella plumes, Journal of volcanology

10 and geothermal research, 70, 169–181, 1996.

Hunt, W. H., Winker, D. M., Vaughan, M. A., Powell, K. A., Lucker, P. L., and Weimer, C.: CALIPSO Lidar Description and Performance Assessment, J. Atmos. Ocean. Tech., 26, 1214–1228, 2009.

James, M., Gilbert, J., and Lane, S.: Experimental investigation of volcanic particle aggregation in the absence of liquid phase, Journal of Geophysical Research, 107, 2191, doi:10.1029/2001JB000950, 2002.

15 James, M., Lane, S., and Gilbert, J.: Density, construction, and drag coefficient of electrostatic volcanic ash aggregates, Journal of Geophysical Research, 108, 2435, doi:10.1029/2002JB002011, 2003.

Johnson, C., Hogg, A., Huppert, H., Sparks, R., Phillips, J., Slim, A., and Woodhouse, M.: Modelling Intrusions through quiescent and moving ambients, Journal of Fluid Mechanics, 771, 370 – 406, doi:10.1017/jfm.2015.180, 2015.

Jones, A., Thomson, D., Hort, M., and Devenish, B.: The UK Met Office's next-generation atmospheric dispersion model, NAME III, in: Air

20 Pollution Modeling and its Application XVII, pp. 580–589, Springer, 2007.

Kristiansen, N., Stohl, A., Prata, A., Richter, A., Eckhardt, S., Seibert, P., Hoffmann, A., Ritter, C., Bitar, L., Duck, T., et al.: Remote sensing and inverse transport modeling of the Kasatochi eruption sulfur dioxide cloud, Journal of Geophysical Research: Atmospheres (1984–2012), 115, 2010.

Mastin, L.: A user-friendly one-dimensional model for wet volcanic plumes, Geochemistry, Geophysics, Geosystems, 8, Q03 014,

25 doi:10.1029/2006GC001455, 2007.

Mastin, L., Guffanti, M., Servranckx, R., Webley, P., Barsotti, S., Dean, K., Durant, A., Ewert, J., Neri, A., Rose, W., et al.: A multidisciplinary effort to assign realistic source parameters to models of volcanic ash-cloud transport and dispersion during eruptions, Journal of Volcanology and Geothermal Research, 186, 10–21, 2009.

Morton, B., Taylor, G., and Turner, J.: Turbulent Gravitational Convection from Maintained and Instantaneous Sources, Proceedings of the

30 Royal Society of London. Series A. Mathematical and Physical Sciences, 234, 1–23, doi:10.1098/rspa.1956.0011, 1956.

Moxnes, E. D., Kristiansen, N. I., Stohl, A., Clarisse, L., Durant, A., Weber, K., and Vogel, A.: Separation of ash and sulfur dioxide during the 2011 Grímsvötn eruption, Journal of Geophysical Research: Atmospheres, 119, 7477–7501, 2014.

Papanicolaou, P. and List, E.: Investigations of round vertical turbulent buoyant jets., Journal of Fluid Mechanics, 195, 341–391, doi:10.1017/S0022112088002447, 1988.

35 Petersen, G., Bjornsson, H., Arason, P., and Löwis, S. v.: Two weather radar time series of the altitude of the volcanic plume during the May 2011 eruption of Grímsvötn, Iceland, Earth System Science Data Discussions, 5, 281–299, 2012.

Prata, A.: Satellite detection of hazardous volcanic clouds and the risk to global air traffic, Natural hazards, 51, 303–324, 2009.

Prata, A. and Bernardo, C.: Retrieval of volcanic SO2 column abundance from Atmospheric Infrared Sounder data, Journal of Geophysical Research: Atmospheres (1984–2012), 112, 2007.

Prata, A. and Grant, I.: Retrieval of microphysical and morphological properties of volcanic ash plumes from satellite data: Application to Mt Ruapehu, New Zealand, Quarterly Journal of the Royal Meteorological Society, 127, 2153–2179, 2001.

Prata, A. and Prata, A.: Eyjafjallajökull volcanic ash concentrations determined using Spin Enhanced Visible and Infrared Imager measurements, Journal of Geophysical Research: Atmospheres (1984–2012), 117, 2012.

Prata, A. J., Gangale, G., Clarisse, L., and Karagulian, F.: Ash and sulfur dioxide in the 2008 eruptions of Okmok and Kasatochi: Insights from high spectral resolution satellite measurements, Journal of Geophysical Research: Atmospheres, 115, n/a–n/a, doi:10.1029/2009JD013556, 2010.

Prata, A. T., Siems, S. T., and Manton, M. J.: Quantification of volcanic cloud top heights and thicknesses using A-train observations for the 2008 Chaitén eruption, J. Geophys. Res. Atmos., 120, 2928–2950, 2015.

Rienecker, M. M., Suarez, M. J., Todling, R., Bacmeister, J., Takacs, L., Liu, H. C., Gu, W., Sienkiewicz, M., Koster, R. D., Gelaro, R., Stajner, I., and Nielsen, J. E.: The GEOS-5 Data Assimilation System— Documentation of Versions 5.0.1, 5.1.0, and 5.2.0, Technical Report Series on Global Modeling and Data Assimilation, 27, NASA/TM-2008-104606, 1–118, 2008.

Robock, A.: Volcanic eruptions and climate, Reviews of Geophysics, 38, 191–219, 2000.

Self, S. and Rampino, M. R.: The 1883 eruption of Krakatau, Nature, 294, 699–704, 1981.

Sparks, R.: The dimensions and dynamics of volcanic eruption columns, Bulletin of Volcanology, 48, 3–15, doi:10.1007/BF01073509, 1986.

Sparks, R., Bursik, M., Carey, S., Gilbert, J., Glaze, L., Sigurdsson, H., and Woods, A.: Volcanic Plumes, John Wileys & Sons, 1997a.

Sparks, R. S. J., Bursik, M., Carey, S., Gilbert, J., Glaze, L., Sigurdsson, H., and Woods, A.: Volcanic plumes, Wiley, 1997b.

Stevenson, J. A., Loughlin, S., Rae, C., Thordarson, T., Milodowski, A. E., Gilbert, J. S., Harangi, S., Lukács, R., Höjgaard, B., Árting, U., Pyne-O'Donnell, S., MacLeod, A., Whitney, B., and Cassidy, M.: Distal deposition of tephra from the Eyjafjallajökull 2010 summit eruption, Journal of Geophysical Research: Solid Earth, 117, n/a–n/a, doi:10.1029/2011JB008904, 2012.

Stohl, A., Prata, A. J., Eckhardt, S., Clarisse, L., Durant, A., Henne, S., Kristiansen, N. I., Minikin, A., Schumann, U., Seibert, P., Stebel, K., Thomas, H. E., Thorsteinsson, T., Tørseth, K., and Weinzierl, B.: Determination of time- and height-resolved volcanic ash emissions and their use for quantitative ash dispersion modeling: the 2010 Eyjafjallajökull eruption, Atmospheric Chemistry and Physics, 11, 4333–4351, doi:10.5194/acp-11-4333-2011, 2011.

Telling, J. and Dufek, J.: An experimental evaluation of ash aggregation in explosive volcanic eruptions, Journal of Volcanology and Geothermal Research, 209–210, 1–8, doi:10.1016/j.jvolgeores.2011.09.008, 2012.

Telling, J., Dufek, J., and Shaikh, A.: Ash aggregation in explosive volcanic eruptions, Geophysical Research Letters, 40, 2355–2360, doi:10.1002/grl.50376, 2013a.

Telling, J., Dufek, J., and Shaikh, A.: Ash aggregation in explosive volcanic eruptions, Geophys. Res. Lett., 40, 2355–2360, 2013b.

Textor, C., Graf, H.-F., Herzog, M., Oberhuber, J. M., Rose, W. I., and Ernst, G. G.: Volcanic particle aggregation in explosive eruption columns. Part I: Parameterization of the microphysics of hydrometeors and ash, Journal of volcanology and geothermal research, 150, 359–377, 2006.

Thomas, H. E. and Prata, A. J.: Sulphur dioxide as a volcanic ash proxy during the April and May 2010 eruption of Eyjafjallajökull Volcano, Iceland, Atmospheric Chemistry and Physics, 11, 6871–6880, doi:10.5194/acp-11-6871-2011, 2011.

Thordarson, T. and Larsen, G.: Volcanism in Iceland in historical time: Volcano types, eruption styles and eruptive history, Journal of Geodynamics, 43, 118–152, 2007.

Thordarson, T. and Self, S.: Atmospheric and environmental effects of the 1783–1784 Laki eruption: a review and reassessment, Journal of Geophysical Research, 108, 4011, 2003.

Tupper, A., Textor, C., Herzog, M., Graf, H.-F., and Richards, M. S.: Tall clouds from small eruptions: the sensitivity of eruption height and fine ash content to tropospheric instability, Natural Hazards, 51, 375–401, doi:10.1007/s11069-009-9433-9, 2009.

Van Eaton, A., Muirhead, J., Wilson, C., and Cimarelli, C.: Growth of volcanic ash aggregates in the presence of liquid water and ice: an experimental approach, Bulletin of Volcanology, 74, 1963–1984, doi:10.1007/s00445-012-0634-9, 2012.

Van Eaton, A., Mastin, L., Herzog, M., Schwaiger, H., Schneider, D., Wallace, K., and Clarke, A.: Hail formation triggers rapid ash aggregation in volcanic plumes, Nature Communications, 6, 1–7, doi:10.1038/ncomms8860, 2015.

Vaughan, M. A., Powell, K. A., Kuehn, R. E., Young, S. A., Winker, D. M., Hostetler, C. A., Hunt, W. H., Liu, Z., McGill, M. J., and Getzewich, B. J.: Fully Automated Detection of Cloud and Aerosol Layers in the CALIPSO Lidar Measurements, J. Atmos. Ocean. Tech., 26, 2034–2050, 2009.

Veitch, G. and Woods, A.: Particle aggregation in volcanic eruption columns, Journal of Geophysical Research: Solid Earth, 106, 26 425–26 441, doi:10.1029/2000JB900343, 2001.

Wen, S. and Rose, W. I.: Retrieval of sizes and total masses of particles in volcanic clouds using AVHRR bands 4 and 5, Journal of Geophysical Research: Atmospheres (1984–2012), 99, 5421–5431, 1994.

Wilson, L. and Huang, T.: The influence of shape on the atmospheric settling velocity of volcanic ash particles, Earth and Planetary Science Letters, 44, 311–324, doi:10.1016/0012-821X(79)90179-1, 1979.

Wilson, L., Sparks, R., Huang, T., and Watkins, N.: The Control of Volcanic Column Heights by Eruption Energetics and Dynamics, Journal of Geophysical Research, 83, 1829–1836, 1978.

Winker, D. M., Liu, Z., Omar, A., Tackett, J., and Fairlie, D.: CALIOP observations of the transport of ash from the Eyjafjallajökull volcano in April 2010, J. Geophys. Res. Atmos., 117, D00U15, 2012.

Woodhouse, M. and Behnke, S.: Charge structure in volcanic plumes: a comparison of plume properties predicted by an integral plume model to observations of volcanic lightning during the 2010 eruption of Eyjafjallajökull, Iceland, Bulletin of Volcanology, 76, doi:10.1007/s00445-014-0828-4, 2014.

Woodhouse, M., Hogg, A., Phillips, J., and Sparks, R.: Interaction between volcanic plumes and wind during the 2010 Eyjafjallajökull eruption, Iceland, Journal of Geophysical Research, 118, doi:10.1029/2012JB009592., 2013a.

Woodhouse, M. J., Hogg, A. J., Phillips, J. C., and Sparks, R. S. J.: Interaction between volcanic plumes and wind during the 2010 Eyjafjallaökull eruption, Iceland, Journal of Geophysical Research: Solid Earth, 118, 92–109, doi:10.1029/2012JB009592, 2013b.

Woods, A.: The fluid dynamics and thermodynamics of eruption columns, Bulletin of Volcanology, 50, 169–193, doi:The fluid dynamics and thermodynamics of eruption columns, 1988.

Woods, A.: Moist Convection and the Injection of Volcanic Ash Into the Atmosphere, Journal of Geophysical Research, 98, 17 627–17 636, doi:10.1029/93JB00718, 1993.

Woods, A. W., Holasek, R. E., and Self, S.: Wind-driven dispersal of volcanic ash plumes and its control on the thermal structure of the plume-top, Bulletin of volcanology, 57, 283–292, 1995.

Yang, K., Krotkov, N. A., Krueger, A. J., Carn, S. A., Bhartia, P. K., and Levelt, P. F.: Retrieval of large volcanic SO_2 columns from the Aura Ozone Monitoring Instrument: Comparison and limitations, Journal of Geophysical Research: Atmospheres (1984–2012), 112, 2007.